NACA RM L57A10

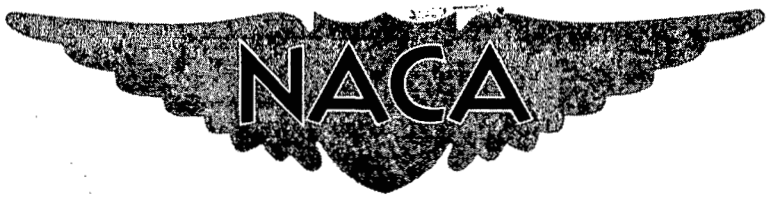

RESEARCH MEMORANDUM

DESIGN AND INVESTIGATION OF A TRANSONIC AXIAL-FLOW COMPRESSOR ROTOR WITH AN INLET HUB-TIP RADIUS RATIO OF ESSENTIALLY ZERO

By Willard R. Westphal and John W. Maynard, Jr.

Langley Aeronautical Laboratory
Langley Field, Va.

NATIONAL ADVISORY COMMITTEE
FOR AERONAUTICS

WASHINGTON

March 11, 1957

NACA RM L57A10

NATIONAL ADVISORY COMMITTEE FOR AERONAUTICS

RESEARCH MEMORANDUM

DESIGN AND INVESTIGATION OF A TRANSONIC AXIAL-FLOW COMPRESSOR ROTOR WITH AN INLET HUB-TIP RADIUS RATIO OF ESSENTIALLY ZERO

By Willard R. Westphal and John W. Maynard, Jr.

SUMMARY

An axial-flow compressor rotor with an inlet hub-tip radius ratio of essentially zero has been designed and investigated in the Langley cascade aerodynamics laboratory. The design specific weight flow was 45.0 pounds per second per square foot of frontal area at a pressure ratio of 1.25 and a tip speed of 1,000 feet per second. The tests showed that the design flow and pressure ratio were attained at design speed at an area-weighted efficiency, including casing boundary layers, of 85 percent. At 120 percent of design speed, a maximum specific weight flow of 46.7 pounds per second per square foot of frontal area was attained.

Low-speed cascade data satisfactorily predicted the flow turning angles in the rotor at relative entering Mach numbers at least up to 1.2.

INTRODUCTION

This paper describes the design of an axial-flow rotor having a design weight flow of 91 percent of choked flow in a duct having a diameter equal to the rotor tip diameter and presents overall performance data.

The advantages of aircraft gas-turbine compressors having a high specific weight flow are well known. Since the thrust is approximately proportional to the weight flow, the thrust per square foot of frontal area is approximately proportional to the specific weight flow. The specific weight flow of axial-flow compressors has steadily increased with time so that now the compressor no longer need be the largest diameter component of a jet engine. Further increases in specific weight flow or decreases in compressor diameter are desirable, however,

since the weight and volume of the engine would then be decreased. Also, increasing the specific weight flow of the front stages of a compressor will increase the blade length of the rear stages. This is beneficial particularly for high-pressure-ratio single-spool compressors which would otherwise have a hub-tip radius ratio greater than 0.9 at the rear stage.

The inlet rotors described in references 1 and 2 having an inlet hub-tip radius ratio of 0.35 have performed well at a specific weight flow of 40.0. This requires an axial Mach number of 0.72 as shown in figure 1. There is little to be gained by increasing the axial Mach number since the weight flow would only increase to 43.4 if the axial Mach number were raised to 1.0. Increasing the axial Mach number would increase the Mach number relative to the rotor and would probably result in lower efficiency at least in the tip region.

The specific weight flow can be increased to about 45.0 at an axial Mach number of 0.765 by decreasing the hub-tip radius ratio from 0.35 to 0.20. In order to demonstrate that rotors of very low hub-tip radius ratio and high mass flow can be designed by conventional aerodynamic methods with slight modifications, a rotor having an inlet hub-tip ratio of 0.0875 has been designed, built, and tested in the Langley cascade aerodynamics laboratory. The design specific weight flow was 45.0 pounds per second per square foot of frontal area. The effective hub-tip ratio was 0.2 after allowance was made for the blockage of the blade roots.

This paper describes the design and the overall performance of this "pinwheel" rotor as determined by testing in Freon-12. The design data presented are for air. The performance data presented were converted to air equivalent values by increasing the velocities by the ratio of the speed of sound in air to that in Freon. Since there is no whirl in the entering flow, both the angle of attack and relative Mach number can be the same in air and Freon at all radii. For the low pressure ratio involved, the difference in the total-pressure rise for air and for Freon is small and has been neglected.

SYMBOLS

A_T/A_1	ratio of minimum width of blade passage to width of entering stream tube
w_e/A_f	equivalent specific weight flow, lb/sec/ft^2 of frontal area at standard atmosphere inlet conditions
M	Mach number
P	total pressure, lb/sq ft

[redacted]

p	static pressure, lb/sq ft
U	rotor speed, ft/sec
β	flow angle measured from axial direction, deg
θ	flow turning angle, deg
η_T	adiabatic efficiency based on measured temperature rise

Subscripts:

1	entering rotor
2	leaving rotor
3	leaving stator
R	relative to rotor
S	stator

DESIGN CONSIDERATIONS

Design of Pinwheel-Type Rotors

The aerodynamic design procedure for a pinwheel-type rotor is not greatly different from that for a rotor of higher inlet hub-tip radius ratio. If there is no swirl in the inlet flow, the flow conditions at the rotor exit may be found without knowing the change of radial position of each streamline through the rotor. The greatest difference is in the greater change of hub radius from inlet to exit of the rotor that is required for the same flow-area contraction, assuming the outer case is not contracted. This leads to a greater slope of the rotor hub and inner case contours. The minimum chord length of the blades and hence the axial width of the rotor are often determined by the desire to keep this slope from becoming excessive. Also, the terms of the radial equilibrium equation that contain the slope and radius of curvature of the streamlines may be so large that they cannot be neglected in calculating the vector diagrams.

The flow-passage contraction must be great enough so that the tangential velocity of the rotor hub at the discharge is a reasonable value. If the hub diameter at discharge is too small, the change in tangential velocity across the rotor, and hence, the tangential velocity entering

[redacted]

the stator, must be very large. This high velocity can be reduced by lowering the design work input at the hub of the rotor as compared with that at the tip. This implies that some later stage must have a higher work input at the hub than at the tip since it is usually required that there be no large radial gradient of total pressure at the discharge of the last stage of the compressor.

The shape of the hub contour that is used to achieve the flow-passage contraction becomes more important as the hub-tip ratio is decreased and the Mach number increased. The shape of the hub contour through a pinwheel rotor no doubt has a considerable effect on the performance of the rotor since the radius change is large and the curvature may be considerable. This is particularly true at flow velocities near sonic. The flow pattern is very sensitive both to area changes and to streamline curvature. Unfortunately, there is no three-dimensional design method by which the optimum hub contour for the transonic regime can be calculated properly, and its selection must be governed by such common-sense considerations as keeping the curvature as low as possible.

Design of the Pinwheel and Stator of Present Investigation

The primary objective in the design of this first pinwheel rotor was to ensure that it would accept the design specific weight flow of 45.0 pounds per second per square foot of frontal area. The design pressure ratio was chosen just high enough to enable the following stator to pass the flow without choking at a hub-tip radius ratio of 0.35. A total-pressure ratio of about 1.25 appeared to be sufficient. This enabled the blade sections to operate at conservative loadings. The design was somewhat influenced by the characteristics of the closed-circuit test rig in which this rotor was to be tested. At the high specific weight flow of the pinwheel rotor, a pressure ratio of about 1.35 is required to overcome the losses in the test loop due to duct turns, cooling radiators, venturi, and so forth. Since the pressure ratio of the pinwheel was to be about 1.25, a booster rotor was necessary. For the sake of expedience, an existing rotor was used as the booster rotor. In order to ensure good performance of the booster rotor, it was specified that its incidence angles be the same as those for which it was originally designed and that the relative Mach number be no higher than in the original design. These conditions required that the radial gradient of work done by the pinwheel be somewhat greater than otherwise necessary. The final design was for a total-pressure ratio of 1.31 at the tip section and 1.18 at the 0.35-radius-ratio section. A tip speed of 1,000 feet per second was selected as a compromise considering blade loading and blade relative Mach numbers.

Selection of vector diagrams.- In computing the vector diagrams, it was assumed that the flow was in simple radial equilibrium between blade rows. A polytropic efficiency of 0.85 based on stagnation conditions was assumed. The radial variation of entropy was neglected. No allowance was made for boundary-layer buildup. An effective inlet hub-tip radius ratio of 0.2 was assumed since it was felt that this would be equal in area to the sum of the frontal area of the actual "nose spinner" and an equivalent frontal area due to the blockage of the blade roots.

The vector diagrams that were computed with this assumption are shown in figure 2. Similar data are presented in table I.

Selection of blade sections.- The selection of blade-section camber and setting angles was based on the low-speed cascade data of references 3 to 5 with no "correction" for Mach numbers or Reynolds number. It was assumed that for the same mean line, camber, solidity, inlet air angle, and angle of attack, the turning angle would be the same in the rotor at transonic Mach numbers and a Reynolds number of 2×10^6 to 3×10^6 as it was in the cascade tunnel at incompressible speeds and a Reynolds number of 0.25×10^6. The design angle of attack was higher than that published as a design value in references 3 and 4 since experience had shown that transonic rotors operated at highest efficiency a few degrees above the low-speed cascade design angle of attack.

The A_6I_{4b} mean line (a moderate loaded-trailing-edge type described in ref. 4) was used for the three outboard blade sections (sections A, B, and C, fig. 3(a)) because it was believed that the portion of the blade having supersonic relative velocities should have only a slight curvature so that the velocity does not increase rapidly in the chordwise direction. The rear portion has lower surface velocities; therefore, the curvature probably should be higher. The A_{10} mean line (symmetrical about the 50-percent-chord line) was used for the inboard rotor blade section (section D in fig. 3(a)). Since there is little difference between upstream and downstream relative Mach numbers near the hub of the pinwheel rotor, the surface curvature should also be the same for the front and the rear of the blade.

The 16-series thickness distribution was used because it had a large cross-sectional area for given maximum thickness and produced a flow-passage area distribution that converged and diverged smoothly. A large cross-sectional area was desirable for the pinwheel because the blades are driven only at the rear inboard portion of each blade and have the highest airload at the forward outboard portion and hence require considerable torsional strength.

[redacted]

Figure 3 shows the shape of the rotor and stator blades. The flow-passage area distribution of several sections of both pinwheel and stator were checked on a two-dimensional basis at constant radii to be sure that no blade section was choked or had a too rapid increase in flow area. The ratio of the throat area to the area of the entering stream tube is shown in table I.

The pinwheel hub was made as small as was structurally practical at the upstream end and kept small for the first 20 percent of axial length of the blades. This was done to reduce the blockage of the hub and blade roots. Since there is very little increase in static density near the hub and a large increase in the tip region of the blade, it was felt that the blockage of the rotor blades would be reduced by allowing some axial distance for the radial flow to occur before increasing the hub radius.

APPARATUS AND INSTRUMENTATION

Rotor Construction

Figure 4 shows the complete pinwheel rotor as tested with the booster rotor. The blades and the forward part of the hub of the pinwheel are made of phenolic resin reinforced with glass fiber. The glass-fiber strands extend from the tip of one blade through the hub and to the tip of the opposite blade in one piece. The steel hub extends forward only to about the 50-percent-chord point of the rotor blades. Two rotors were built with the intention of spin-testing one to destruction to determine the ultimate strength of such rotors. The shaft from which the rotor was suspended in the spin test rig failed at about 60 percent of the aerodynamic design speed for air and dropped the rotor on its upstream face. Two opposite blades appeared to be undamaged and these blades were pulled to failure in a static tensile test with the hub unsupported. The blades parted at the axis of the rotor at a tensile load equal to 160 percent of the calculated centrifugal force at design speed in air. The strength could probably be improved considerably by threading the glass-fiber strands at the rotor axis in smaller groups. The strands were gathered into four groups at the rotor axis of the blade that failed.

Since the safety factor was marginal, the second rotor was tested only in Freon-12 and not in air.

Instrumentation

Figure 5(a) is a plan view of the test loop. Figure 5(b) is a section of the test section showing the instrument locations.

The overall performance of the rotor was measured by fixed instrumentation located as follows:

(a) Two rakes (fig. 6), each measuring both total temperature and total pressure, one upstream and one downstream of the rotor as indicated in figure 5(b)

(b) Six static orifices equally spaced circumferentially in the outer casing at each of the instrument stations

(c) One static-pressure probe 0.060-inch in diameter on the rotor axis with four orifices 1.1 inches forward of the nose of the rotor

Weight flow was measured by calibrated venturi. The location of the rakes was found to have a large effect on the flow measurements. The rotor's performance had been first measured with the usual type of instrumentation, that is, separate rakes for total-temperature and total-pressure measurements at the same axial station but at different circumferential locations. It was found that this resulted in very large circumferential gradients of pressure and temperature which made it impossible to determine accurately the rotor's performance, particularly its efficiency. Efficiencies as high as 120 percent were calculated from measurements of total pressure and temperature by rakes of the same frontal area located 90° apart downstream of the rotor.

The data presented in this report are based on total-pressure and total-temperature measurements that were made along the same radial line by use of the combined pressure and temperature rakes shown in figure 6. The upstream and downstream rakes were located along the same axial line so that small variations in the temperature of the entering flow did not appreciably affect the efficiency determination. The flow path through the rotor is curved enough so that the wake of the upstream instrument does not impinge on the downstream instrument.

The total-pressure orifices were made by drilling out the 0.060-outer-diameter tubing to an inner diameter of 0.050 for a depth of 0.060 inch. Such an orifice should give a true total pressure for flow incidence angles of $\pm 15^{\circ}$ (ref. 6). The rake was set at the mean angle of the flow.

Detailed survey data were obtained with the instrument shown in figure 6.

[redacted]

Test Procedure

The total-pressure ratio, total-temperature rise, and weight flow were measured over the range of throttle positions at air equivalent corrected speeds of 60, 80, 90, 95, 100, 105, 110, and 120 percent of design speed. For these tests, the only instruments in the airstream were the two combined temperature and pressure rakes.

Some survey data were taken at design speed. For these tests, the combined rakes were removed and the survey instrument shown in figure 6 was traversed across the passage upstream and downstream of the rotor at different times to minimize the flow-blockage effect of the instrument. The two sets of data were correlated on the basis of the average weight flow as measured by the venturi.

No data were taken on the performance of the stator blades or the booster rotor.

RESULTS AND DISCUSSION

The radial distribution of total-pressure ratio and efficiency are plotted in figures 7 and 8, respectively. The measured pressure ratio at design speed has a steeper radial gradient than the design values which are shown as a solid line in figure 7(e). The rotor's performance falls near the outer casing, particularly at the higher speeds, as is usually the case. The rotor tip's performance is not well defined since there is only one total-pressure orifice (0.18 inch from the casing) that is, in the tip-loss region. The next orifice (0.72 inch from the casing) is completely out of the tip-loss region and so does not give much information on the extent of this region.

The pressure ratio near the inner casing is less than 1 indicating that the flow has high losses and is separated or nearly separated from the casing for the open throttle positions at speeds of design and higher (figs. 7(e) to (h)). This loss region is reduced by throttling the compressor as is usually the case where the losses are due to shock-induced separation. In the case of the hub section of the pinwheel, the supersonic flow on the blade surface is increased by the short radius of curvature of the rotor hub as shown in figure 3(a) and is further increased by the increase in the axial Mach number of the flow when the back pressure is reduced. The static-pressure rise across the hub section of the rotor is low at all flow conditions so that it is not likely to have an important effect on the rotor hub-section performance. The hub-section performance could probably be improved by reducing the curvature of the rotor surface.

The efficiencies shown in figure 8 are plotted at the radius of the total-pressure orifice. The total-temperature rise at that radius was obtained from faired plots of the measured temperature rise against radius.

At design speed and below, the efficiency is above 90 percent at all weight flows except at the hub and tip regions where the efficiency falls markedly (figs. 8(a) to (e)).

The overall performance of the pinwheel rotor is shown in figure 9. The total-pressure ratio (fig. 9(a)) and efficiency (fig. 9(b)) are area weighted, not mass weighted, and include the casing boundary layers at hub and tip. This results in lower values than those obtained by mass-weighting and omitting the boundary layers. Design weight flow and pressure ratio were achieved at the design speed. The axial Mach number entering the blade row as computed from casing static pressure and settling-chamber total pressure also agrees with the design value of 0.76. This implies that the blades are operating at the design angle of attack, of course, and also that the rather arbitrary estimate of the blockage of the blade roots and the hub of the rotor at the inlet was correct. An effective hub-tip radius ratio of 0.2 was assumed in the design. The actual hub-tip ratio of the nose spinner is 0.087.

The weight flow continued to increase as speed was increased above the design value. The highest specific weight flow attained was 46.7 pounds per second per square foot at 120 percent of design speed. At this weight flow the inlet axial Mach number was 0.87.

The surge line in figure 9(a) indicates the lowest weight flow attained without audible unsteadiness of the flow. It is not known which of the three blade rows stalled first.

The dashed line is a line of constant tip angle of attack at the design value. It shows that at low speeds the rotor was at a high angle of attack even at the highest weight flow. This is a result of the high losses in the closed-loop test rig. The positive slope of the curve of the variation of efficiency with weight flow for low speeds in figure 9(b) seems to indicate that the optimum angle of attack was only approached at wide-open throttle.

At speeds higher than design, the angles of attack were also high, but not as the result of the test-loop limitations, since the characteristic line is very nearly vertical at the high-flow end of each of these curves. The high angles of attack were probably necessary in order to accept the incoming flow without choking.

The peak overall efficiency was only about 85 percent at design speed and fell rapidly as speed was increased.

[redacted]

The rotor inlet and outlet flow angles are shown in figure 10. The inlet axial velocities were computed from static-pressure measurements at the casing and at the rotor center line and not from a radial survey. The outlet flow angles were computed from survey data.

The outlet flow angles were less than design for all weight flows for the whole passage except at the extreme end. The blading overturned the flow about 2°. This is good agreement considering that the blade cambers and setting angles were selected solely from incompressible cascade data with no corrections for the change of Mach number from 0.1 to 1.0, the change of Reynolds numbers from 0.245×10^6 to approximately 2×10^6 or the change from a two-dimensional cascade to a three-dimensional rotor. Similar results have been obtained with other rotors, both subsonic and transonic, designed from low-speed cascade data. The overturning is usually about 1° to 2°.

The turning angle near the inner casing is greatest at the lower weight flow. This supports the earlier observation that the separation at the hub section is due to the high Mach number flow over the sharply curved rotor hub and not to too rapid diffusion on the blade surface.

SUMMARY OF RESULTS

A compressor rotor of essentially zero inlet hub-tip radius ratio was designed for a specific weight flow of 45.0 pounds per second per square foot area and a pressure ratio of 1.25 at a tip speed of 1,000 feet per second. The following conclusions were drawn from the results of tests of this rotor:

1. The design weight flow and pressure ratio were attained at design speed.

2. Maximum weight flow continued to increase with increasing speed at all speeds tested. A specific weight flow of 46.7 was obtained at 120 percent of design speed.

3. Low-speed cascade data satisfactorily predicted the flow turning angles in the rotor at relative entering Mach numbers at least up to 1.2.

[redacted]

4. Peak area-weighted adiabatic efficiencies, including case boundary layers, at design speed were 85 percent and decreased with increasing speed.

Langley Aeronautical Laboratory,
National Advisory Committee for Aeronautics,
Langley Field, Va., December 17, 1956.

[redacted]

REFERENCES

1. Savage, Melvyn, and Felix, A. Richard: Investigation of a High-Performance Axial-Flow Compressor Inlet Rotor Designed for 37.5 Pounds Per Second Square Foot of Frontal Area - Aerodynamic Design and Overall Performance. NACA RM L55A05, 1955.

2. Boxer, Emanuel, and Bernot, Peter T.: Experimental Investigation of a Transonic Axial-Flow-Compressor Rotor Designed for Sonic Inlet Velocity With an Inlet Hub-Tip Radius Ratio of 0.35. NACA RM L56F14, 1956.

3. Herrig, L. Joseph, Emery, James C., and Erwin, John R.: Systematic Two-Dimensional Cascade Tests of NACA 65-Series Compressor Blades at Low Speeds. NACA TN 3916, 1957. (Supersedes NACA RM L51G31.)

4. Erwin, John R., Savage, Melvyn, and Emery, James C.: Two-Dimensional Low-Speed Cascade Investigation of NACA Compressor Blade Sections Having a Systematic Variation in Mean-Line Loading. NACA TN 3817, 1956. (Supersedes NACA RM L53I30b.)

5. Herrig, L. Joseph, Emery, James C., and Erwin, John R.: Effect of Section Thickness and Trailing-Edge Radius on the Performance of NACA 65-Series Compressor Blades in Cascade at Low Speeds. NACA RM L51J16, 1951.

6. Gracey, William, Letko, William, and Russell, Walter R.: Wind-Tunnel Investigation of a Number of Total-Pressure Tubes at High Angles of Attack - Subsonic Speeds. NACA TN 2331, 1951. (Supersedes NACA RM L50G19.)

TABLE I

Radius, ft	Inlet air angle, deg	Turning angle, deg	Entering Mach number	$\frac{p_2 - p_1}{(P - p)_{entering}}$	Diffusion factor	Camber	Solidity	$\frac{\text{Thickness}}{\text{Chord}}$	Angle of attack, deg	$\frac{A_T}{A_1}$	$\alpha_{des} - \alpha_{des(ref.\ 3)}$, deg
Pinwheel rotor											
0.5	51.0	10.1	1.22	0.20	0.33	0.60	0.75	0.04	8.9	1.13	2.7
.4	44.7	12.6	1.08	.25	.36	.60	.92	.04	9.7	1.08	2.7
.3	36.5	18.5	.955	.29	.38	.74	1.20	.04	12.7	1.05	3.1
.2	26.3	30.9	.88	.21	.33	1.08	1.76				
.175	23.4	34.8	.84	.18	.30	1.28	2.00	.05	22.5		5.0
Stator											
0.5	20.5	10.2	0.78	0.16	0.23	0.64	0.52	0.07	9.3	1.01	4.3
.4	22.6	14.5	.76	.21	.28	.84	.66	.07	11.1	1.00	4.3
.3	26.0	24.3	.75	.31	.36	1.28	.87	.07	15.3	1.00	4.3
.2	32.1	39.1	.80	.48	.41	1.77	1.31	.07	21.8		4.1
.175	34.1	43.1	.83	.49	.48	1.90	1.50	.07	24.2	1.02	5.0

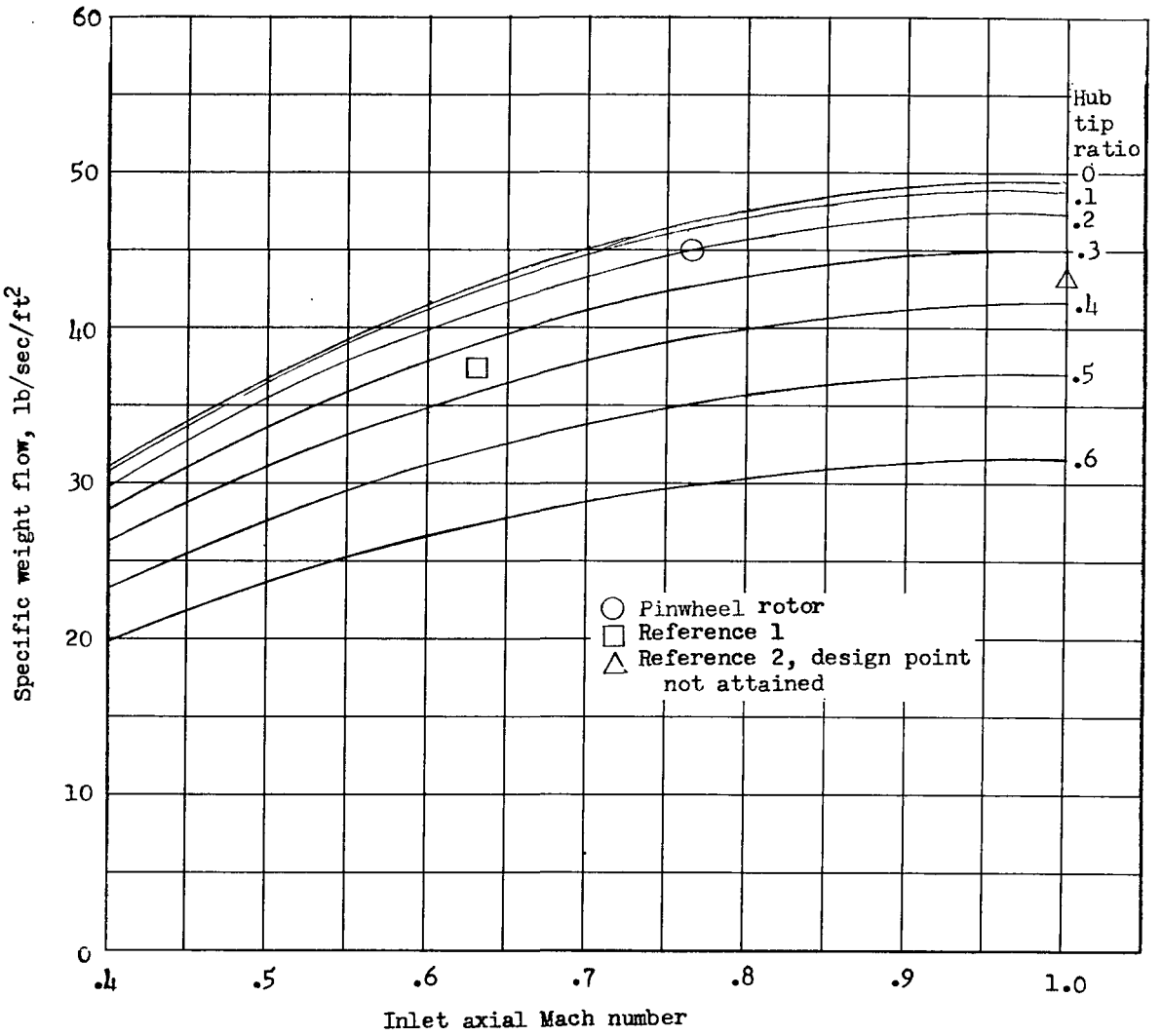

Figure 1.- Specific weight flow against inlet axial Mach number for several hub-tip ratios.

[redacted]

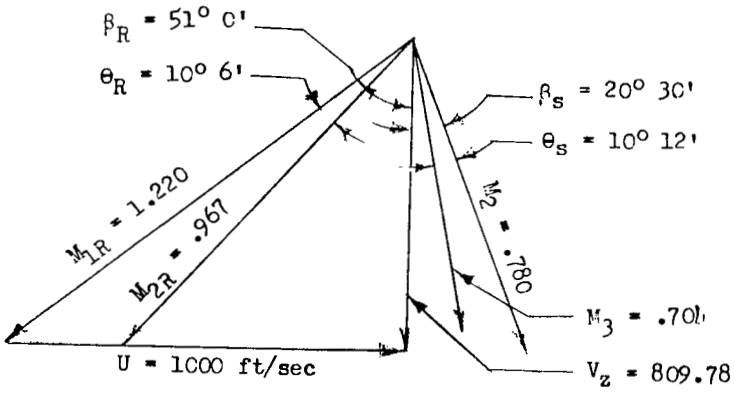

Tip section, radius = 0.5 ft

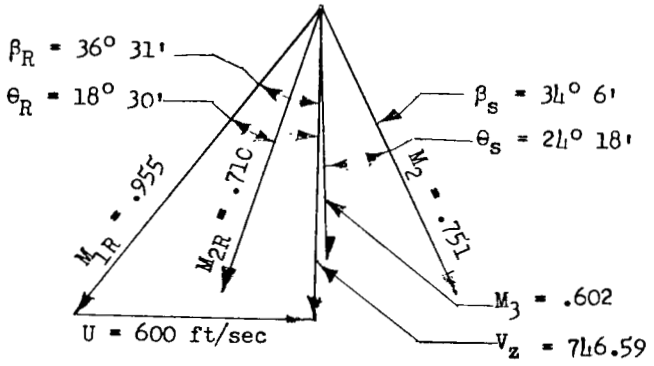

Pitch section, radius = 0.3 ft

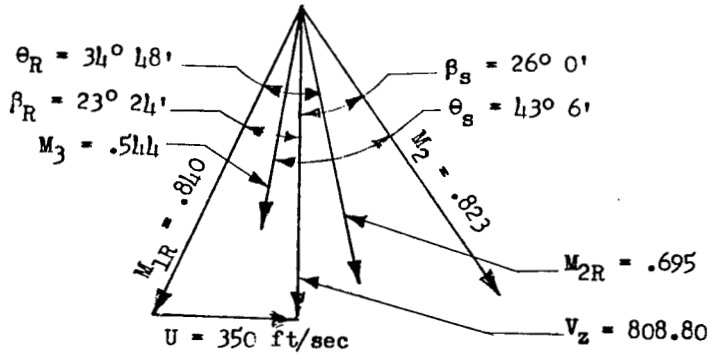

Root section, radius = 0.175 ft

Figure 2.- Design vector diagrams for pinwheel and stator at several radii.

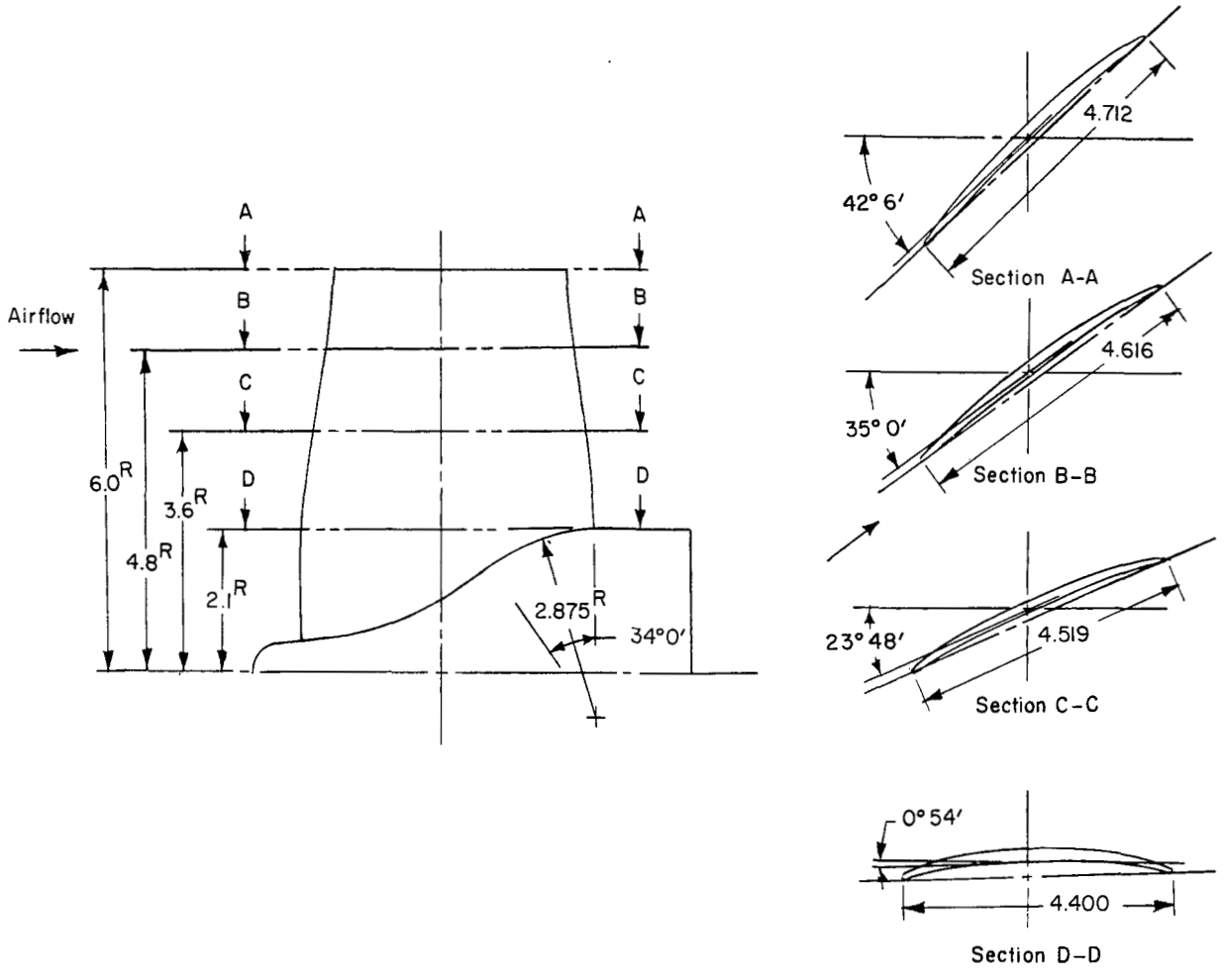

(a) Rotor blade.

Figure 3.- Shape of blades. All dimensions are in inches.

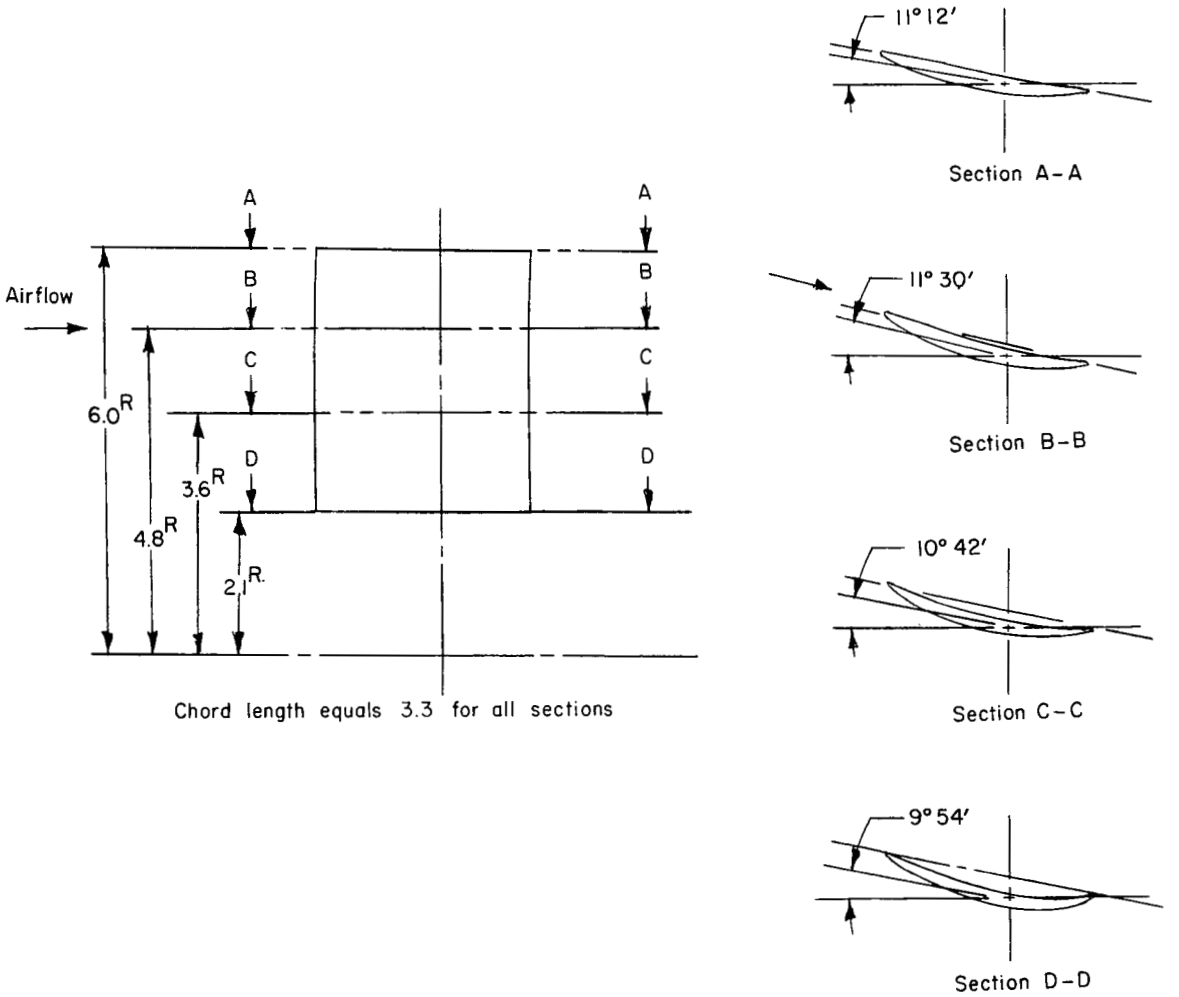

(b) Stator blade.

Figure 3.- Concluded.

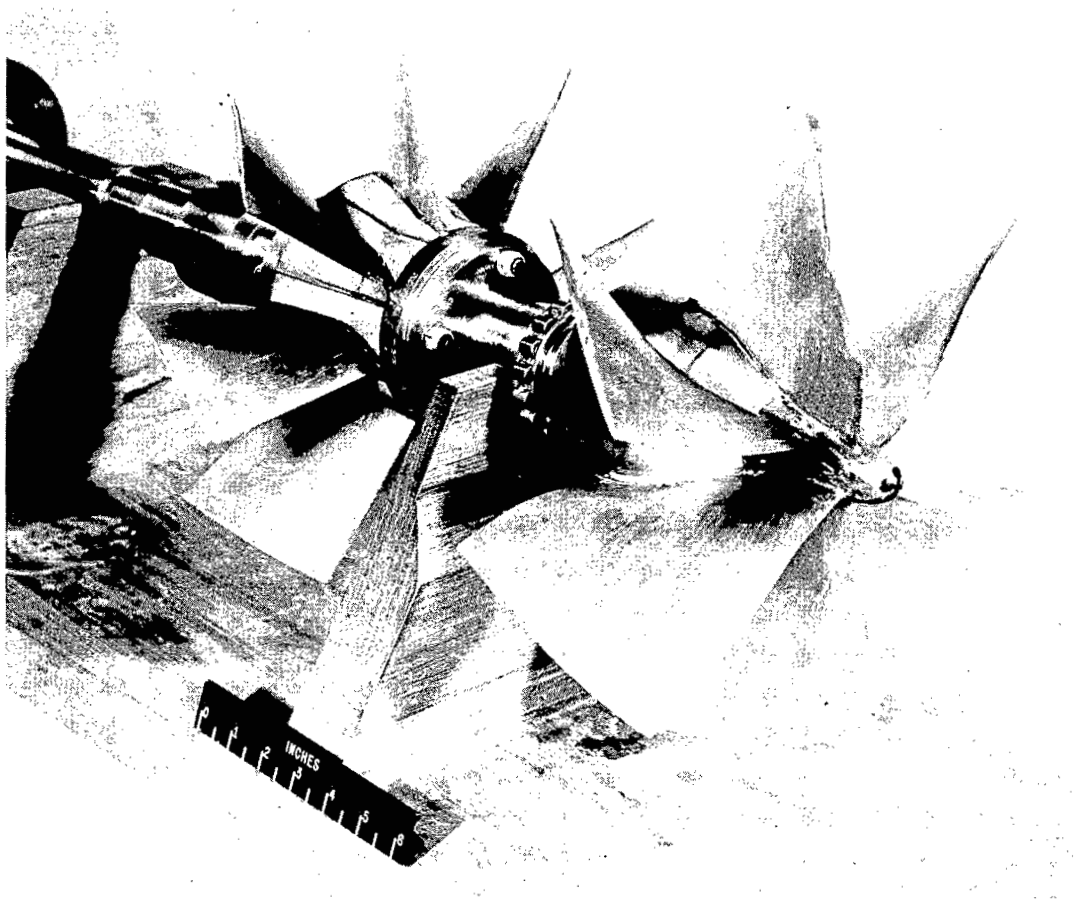

(a) One-quarter front view. L-85442

Figure 4.- Pinwheel and booster rotor assembly.

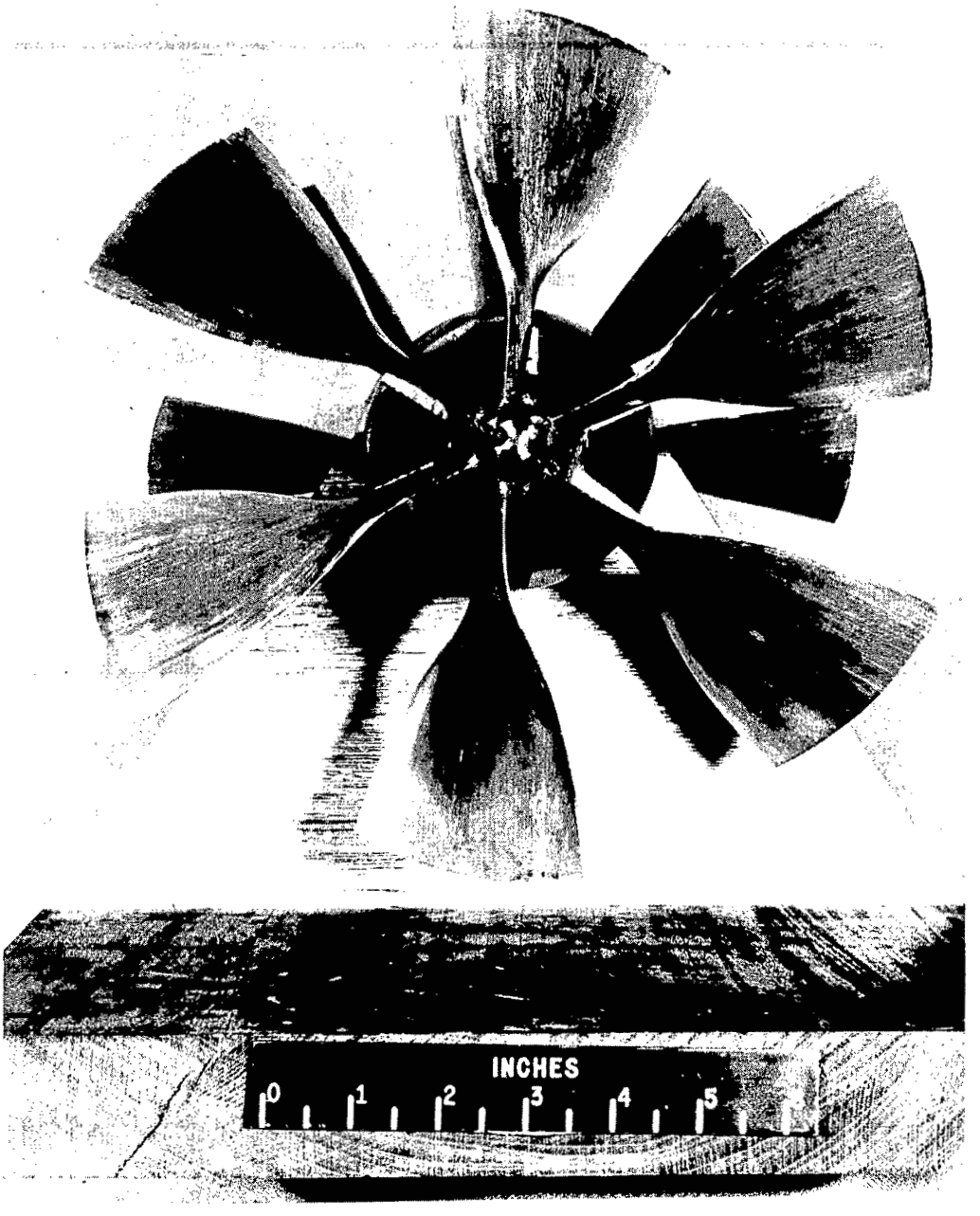

(b) Full front view. L-85443

Figure 4.- Concluded.

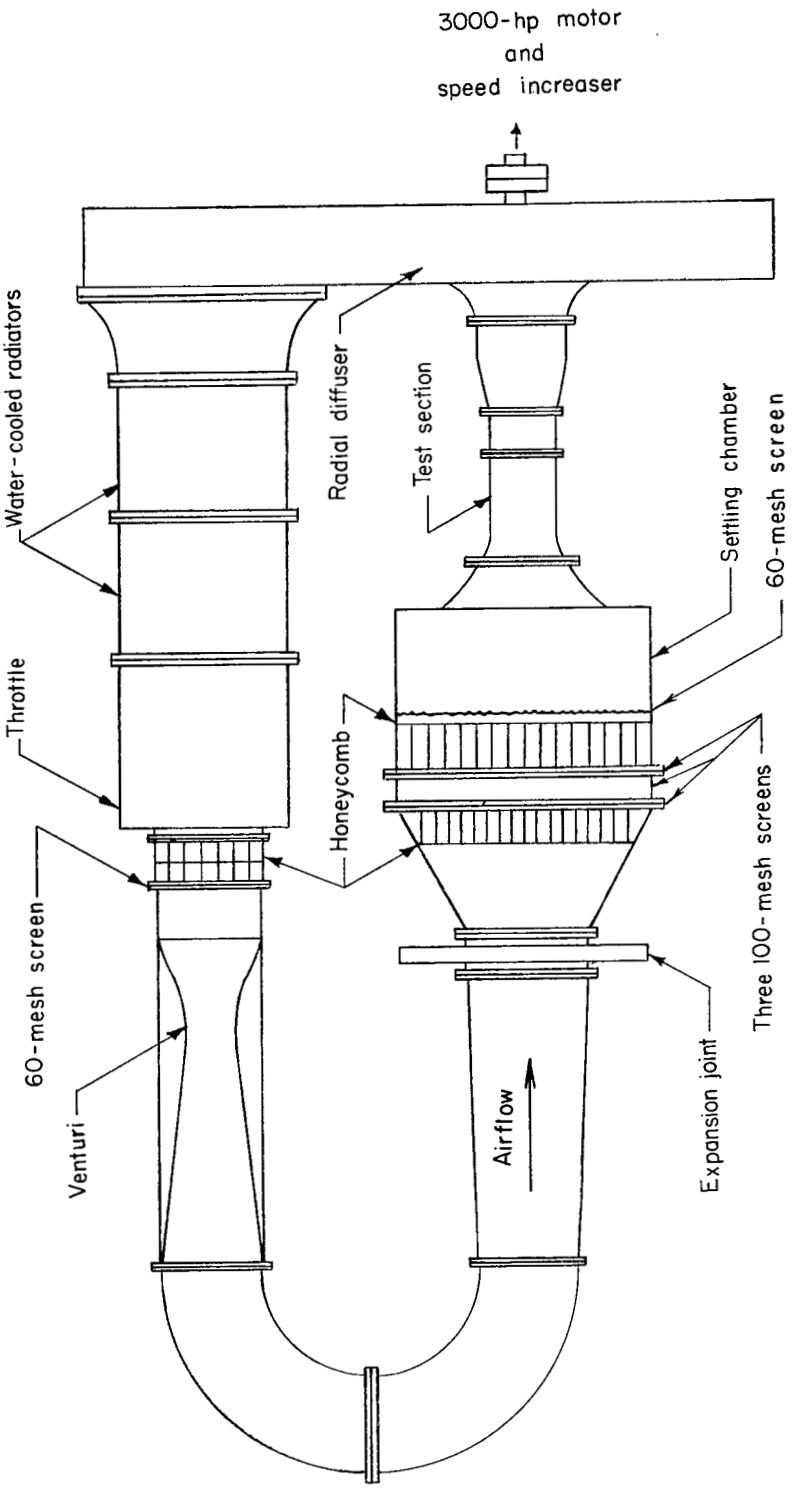

(a) Test loop.

Figure 5.- Schematic diagram of compressor test installation.

[redacted]

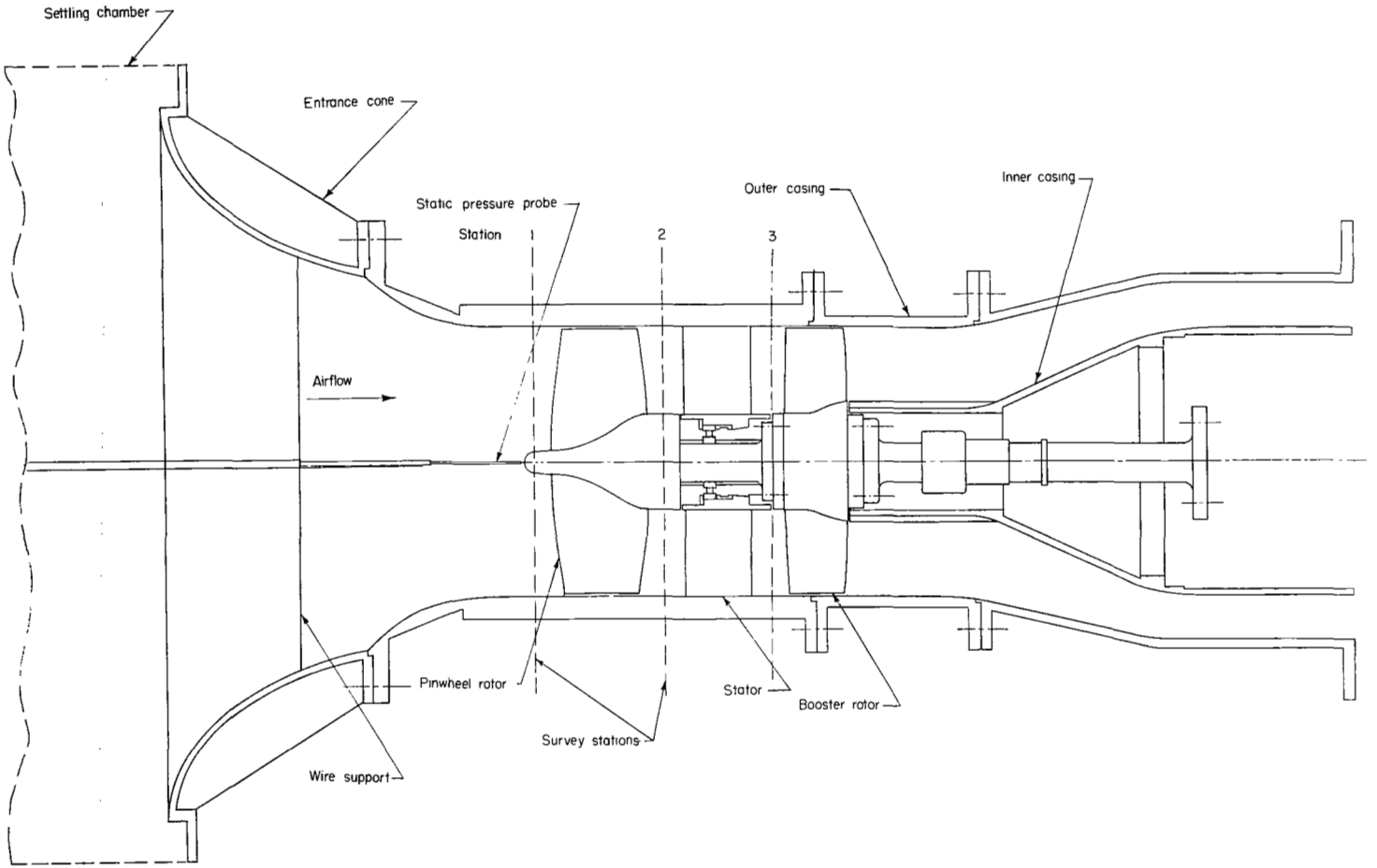

(b) Test section.

Figure 5.- Concluded.

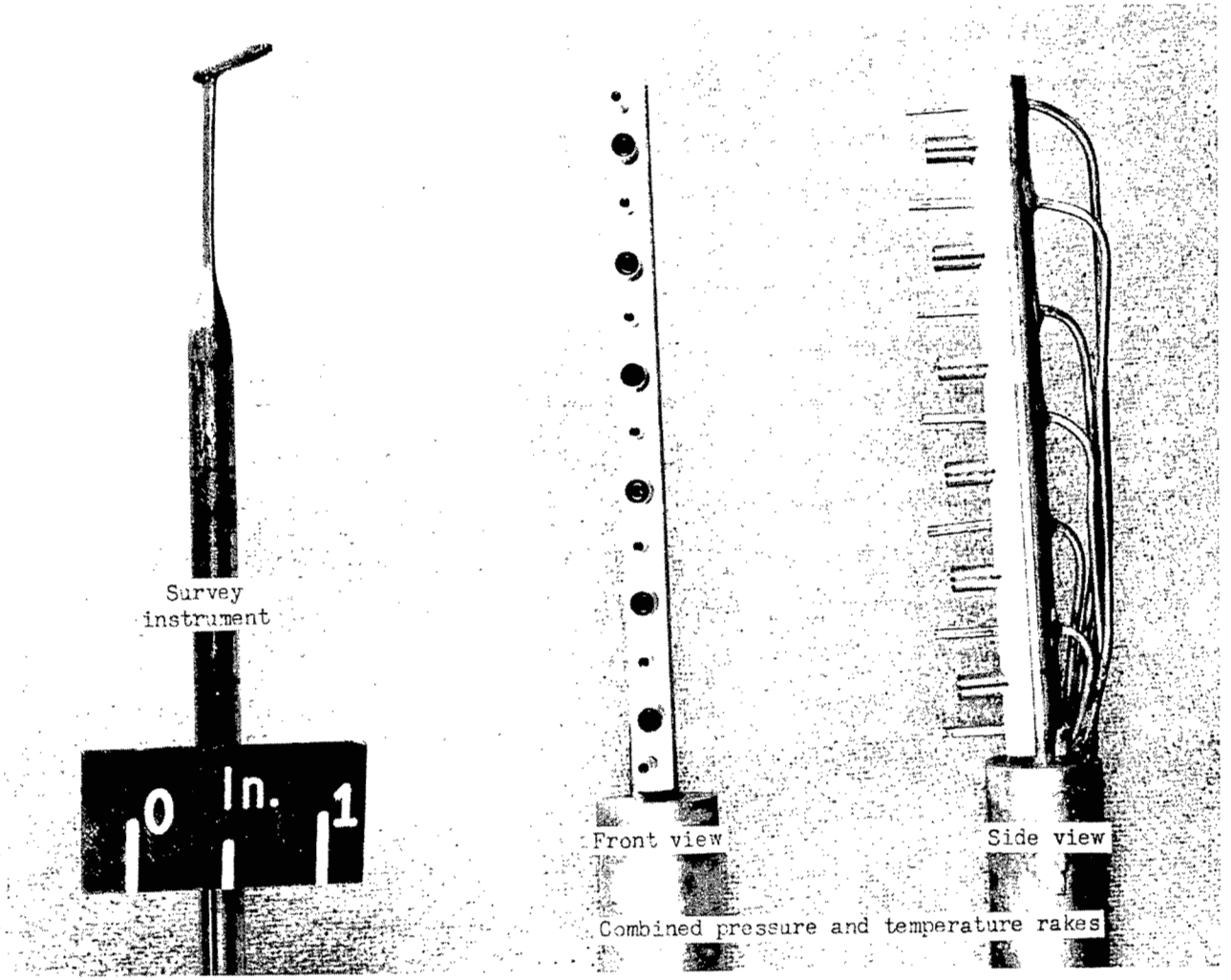

L-91940.1

Figure 6.- Instruments.

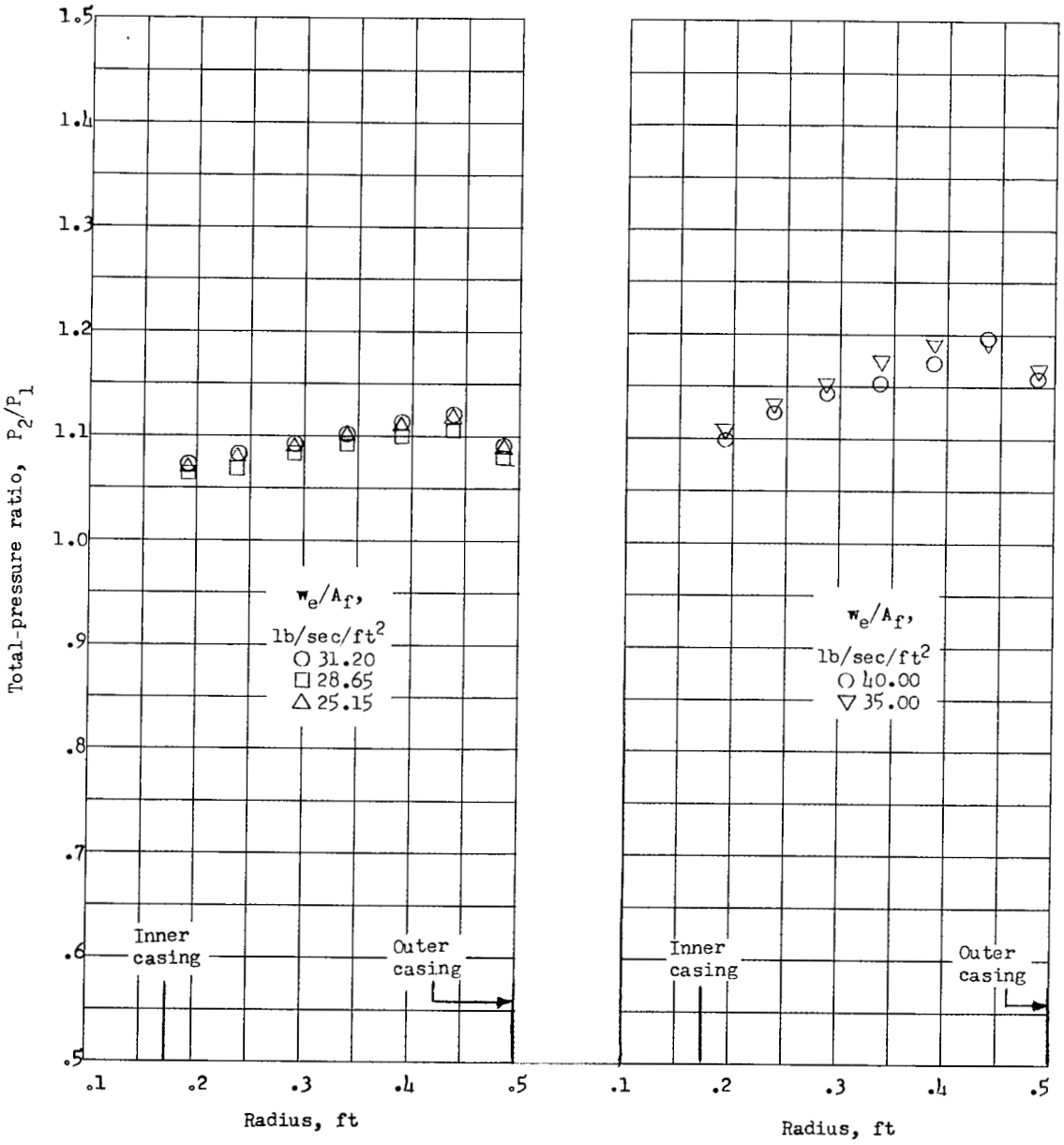

(a) 60-percent design speed.

(b) 80-percent design speed.

Figure 7.- Variation of total-pressure ratio with radius for several weight flows.

[redacted]

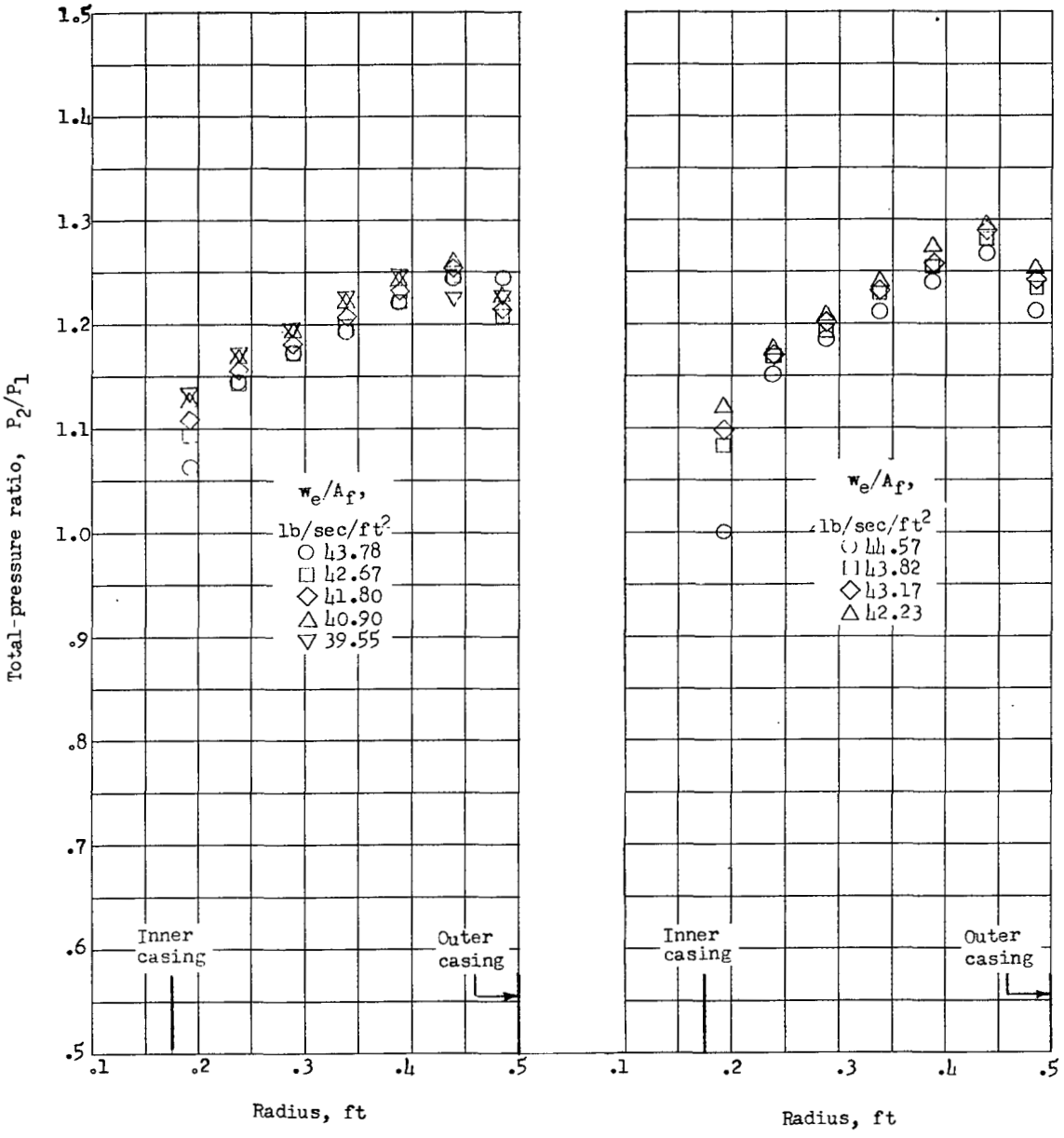

(c) 90-percent design speed.

(d) 95-percent design speed.

Figure 7.- Continued.

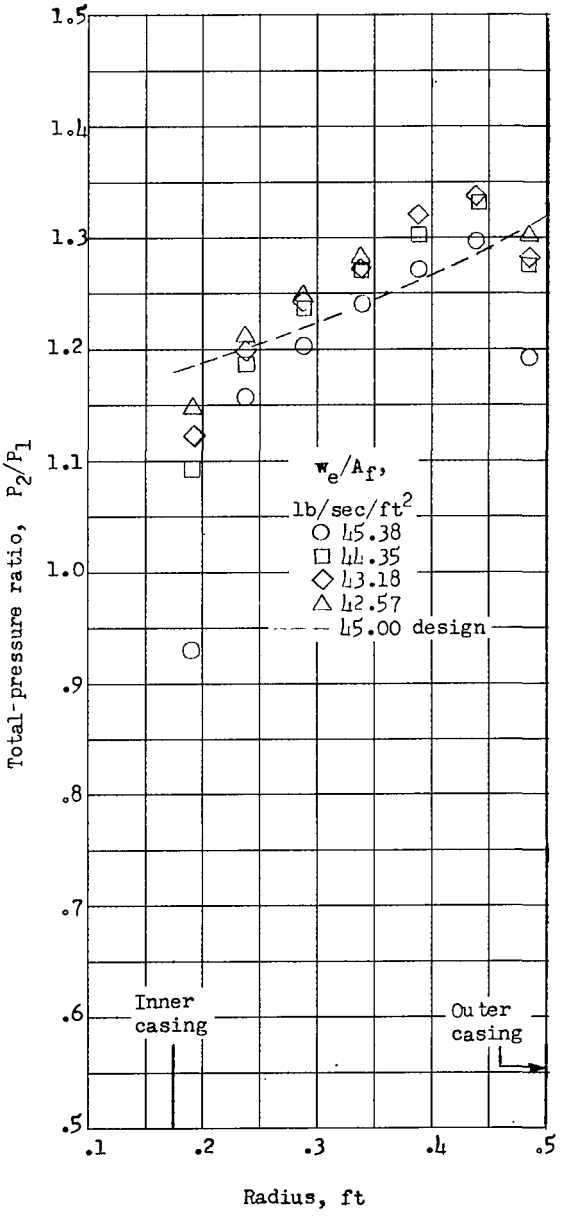

(e) Design speed.

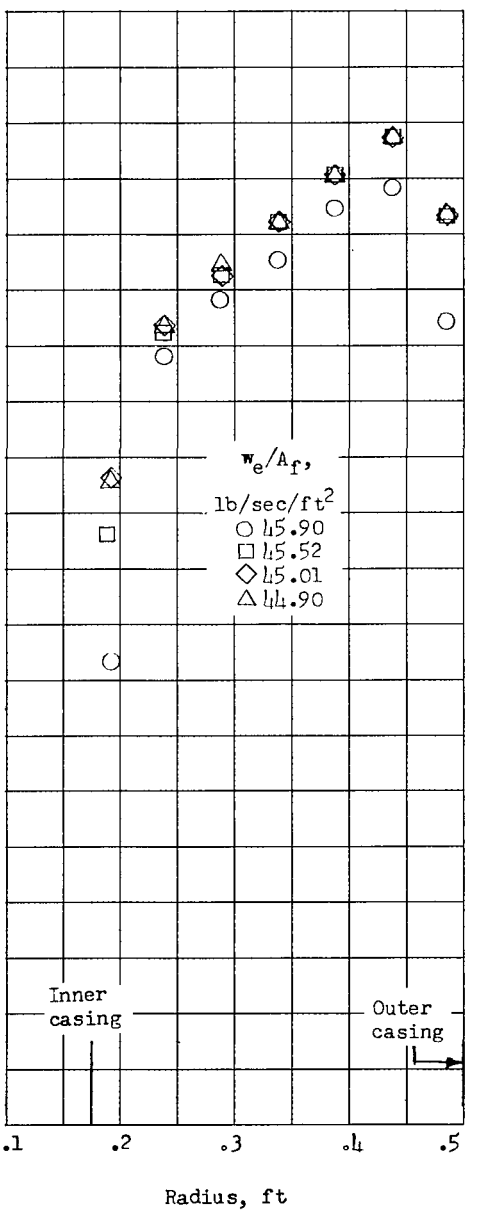

(f) 105-percent design speed.

Figure 7.- Continued.

[redacted]

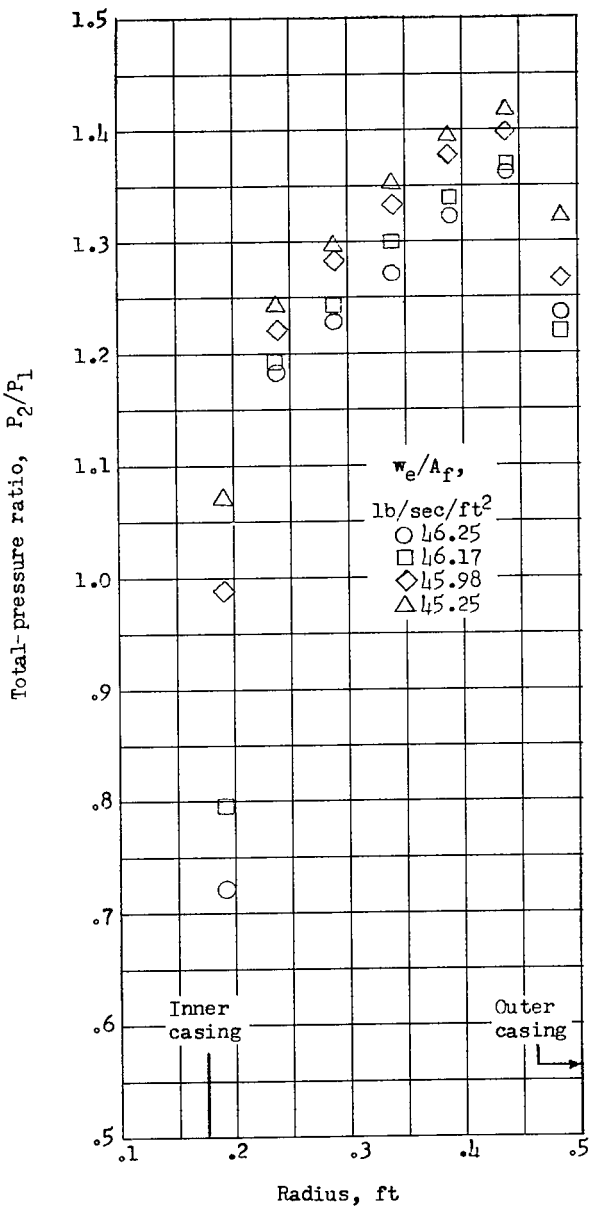

(g) 110-percent design speed.

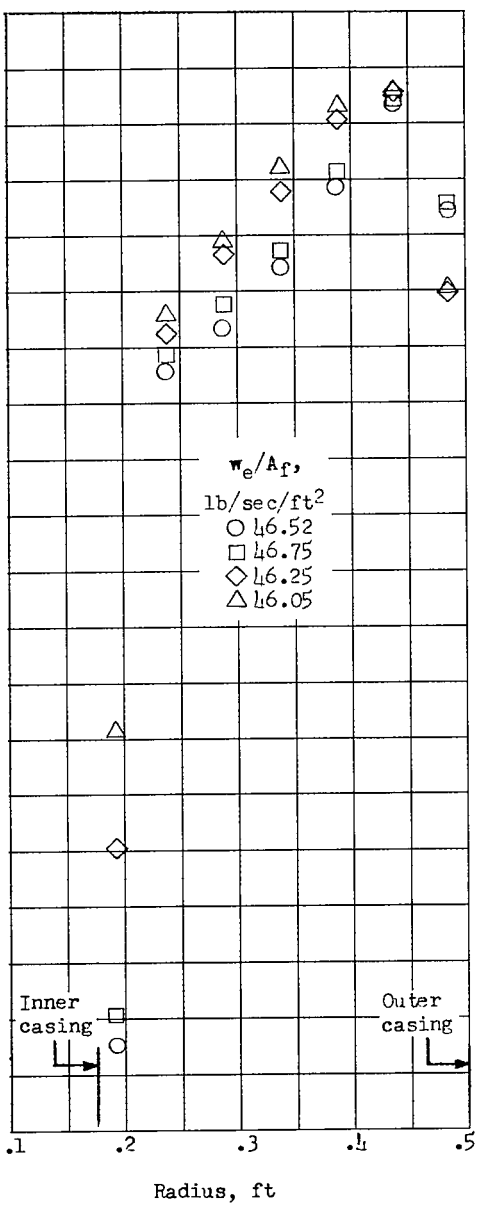

(h) 120-percent design speed.

Figure 7.- Concluded.

[redacted]

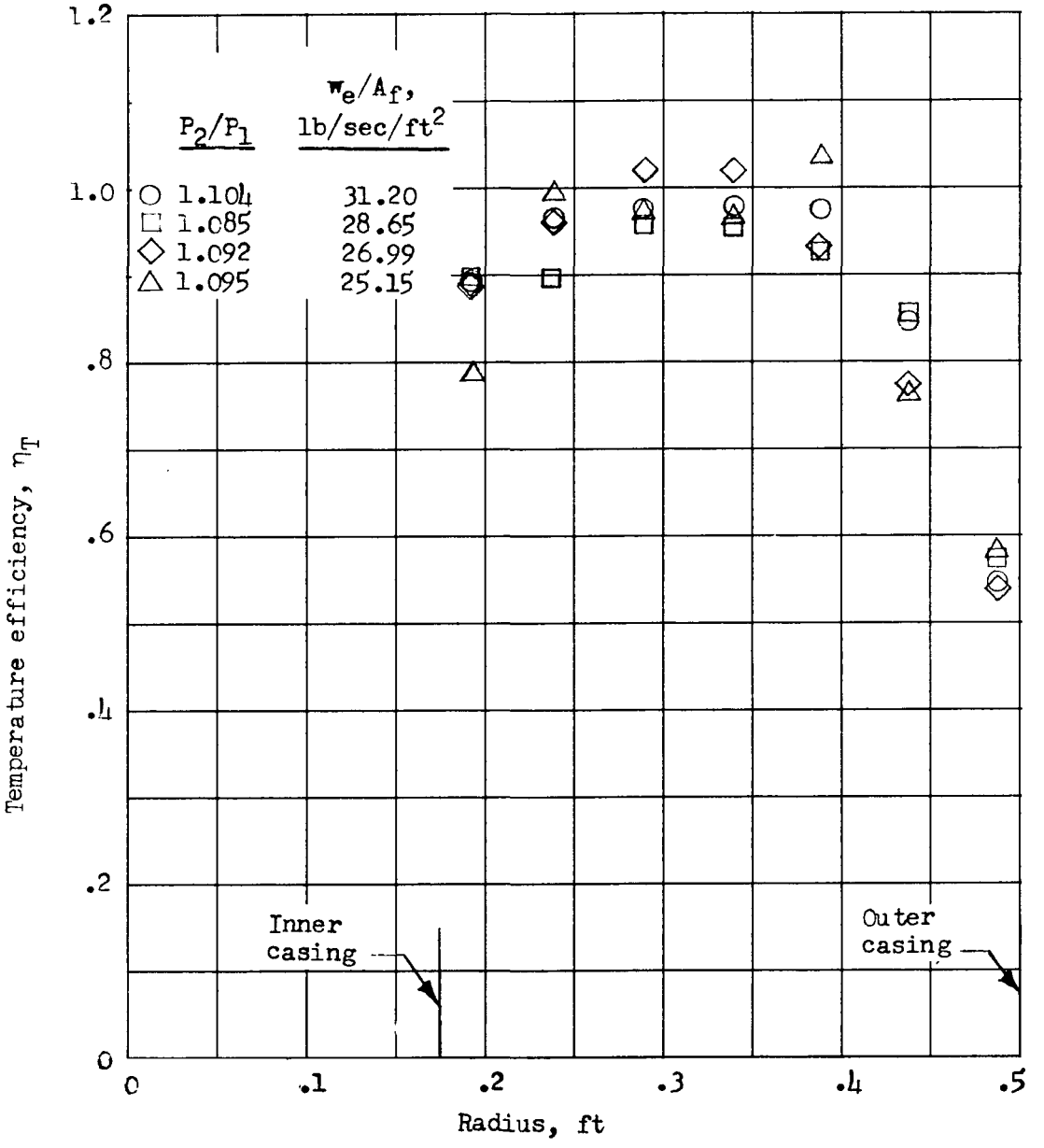

(a) 60-percent design speed.

Figure 8.- Variation of temperature efficiency with radius at several weight flows.

[redacted]

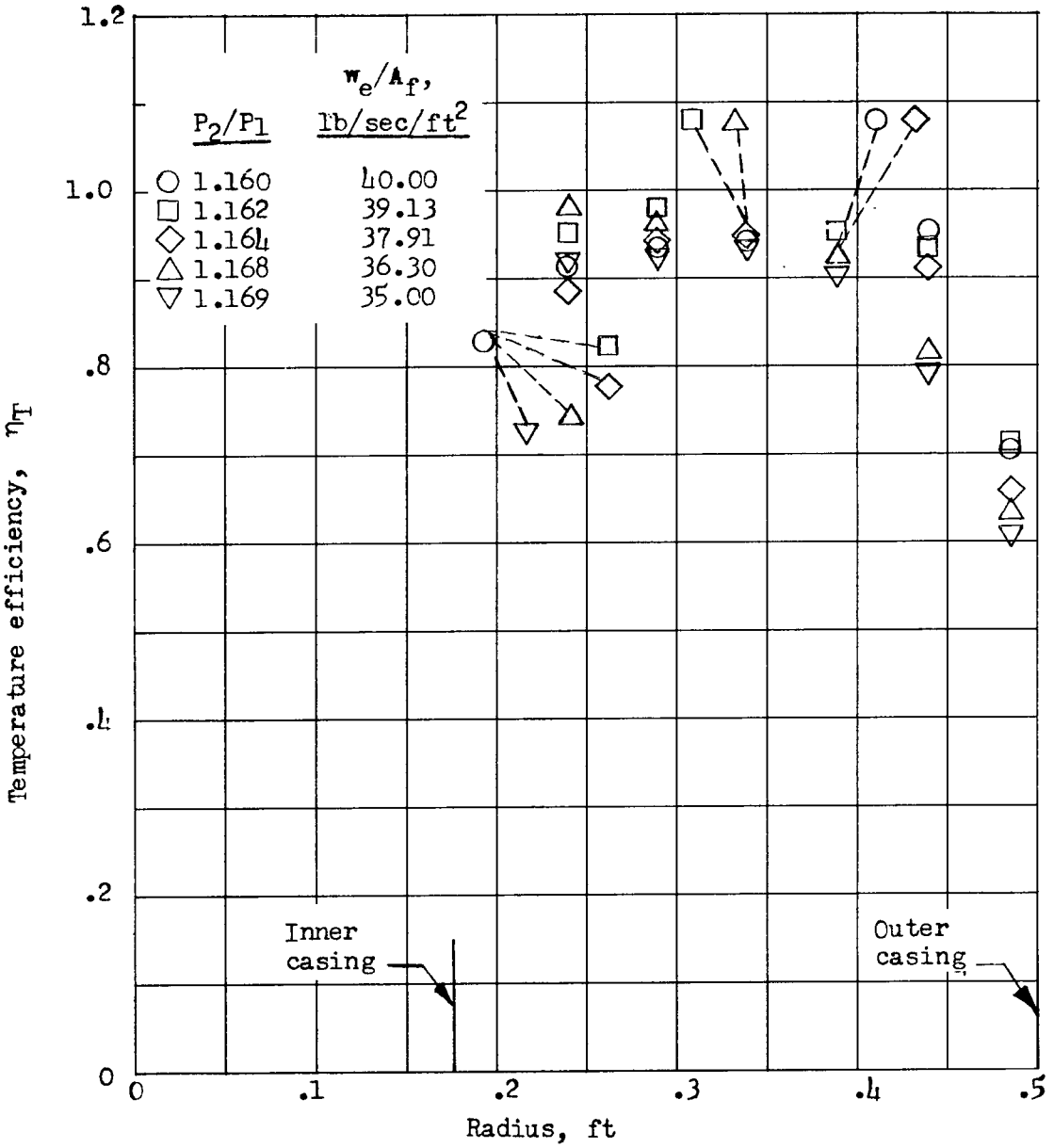

(b) 80-percent design speed.

Figure 8.- Continued.

[redacted]

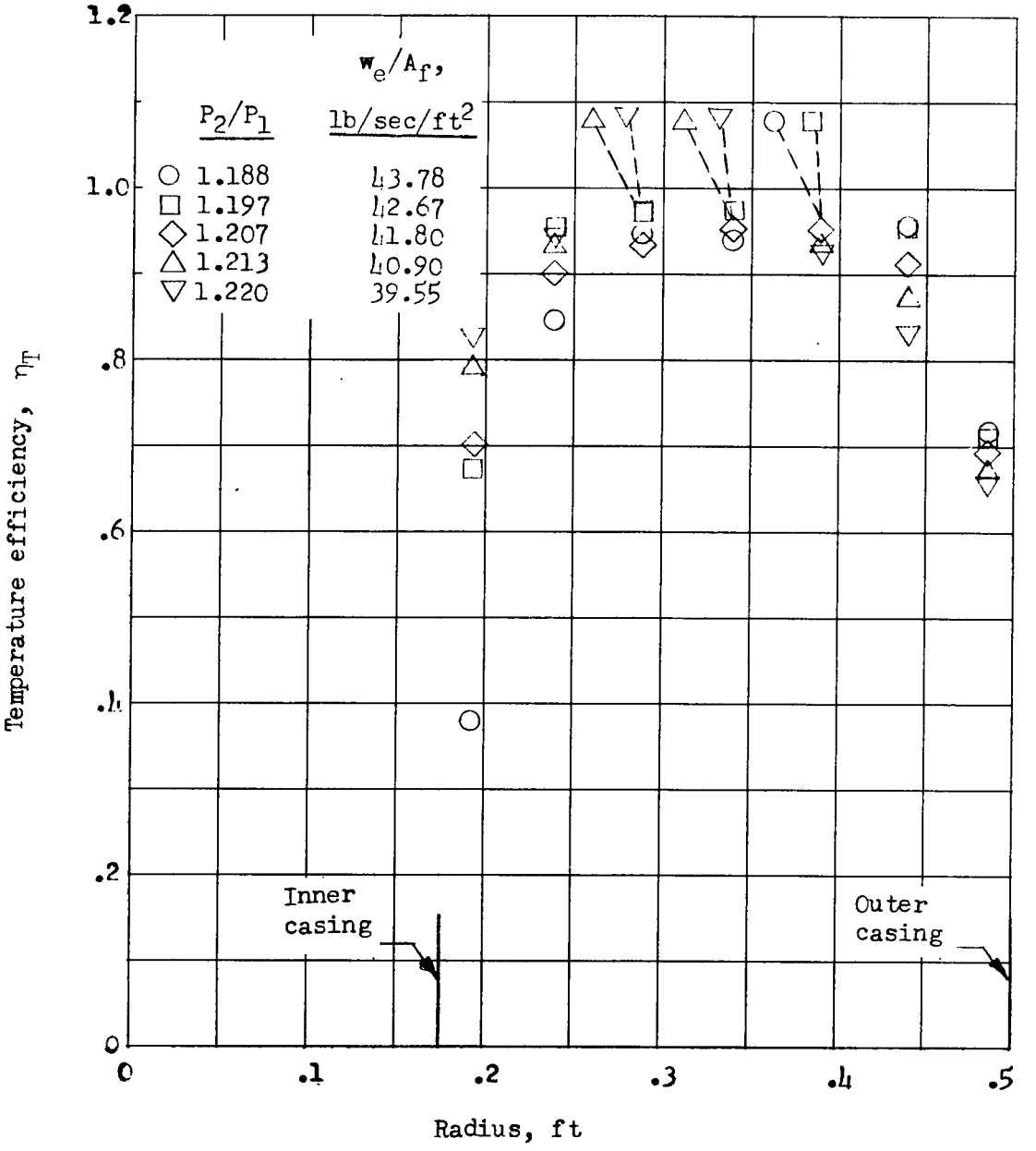

(c) 90-percent design speed.

Figure 8.- Continued.

[redacted]

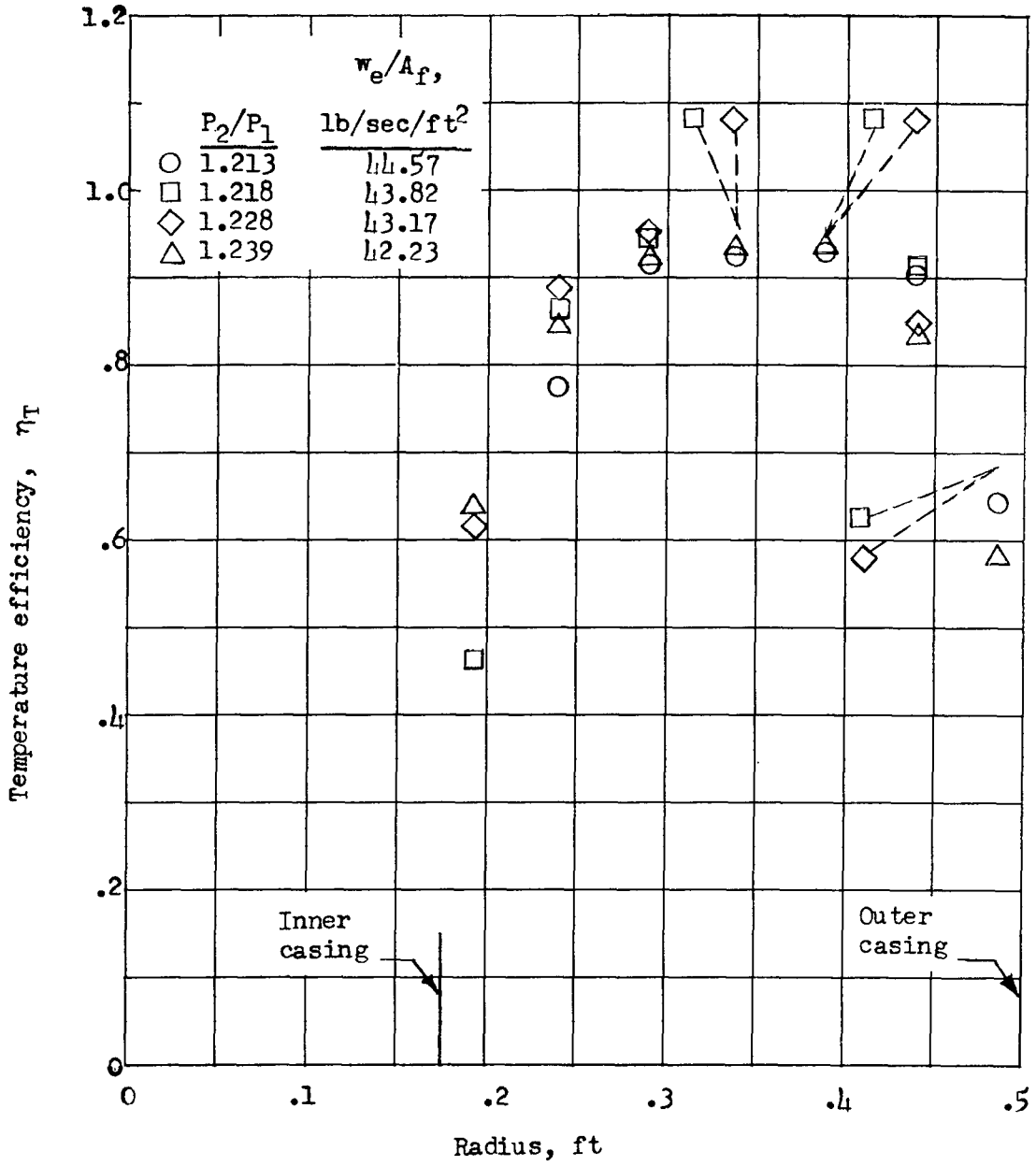

(d) 95-percent design speed.

Figure 8.- Continued.

[redacted]

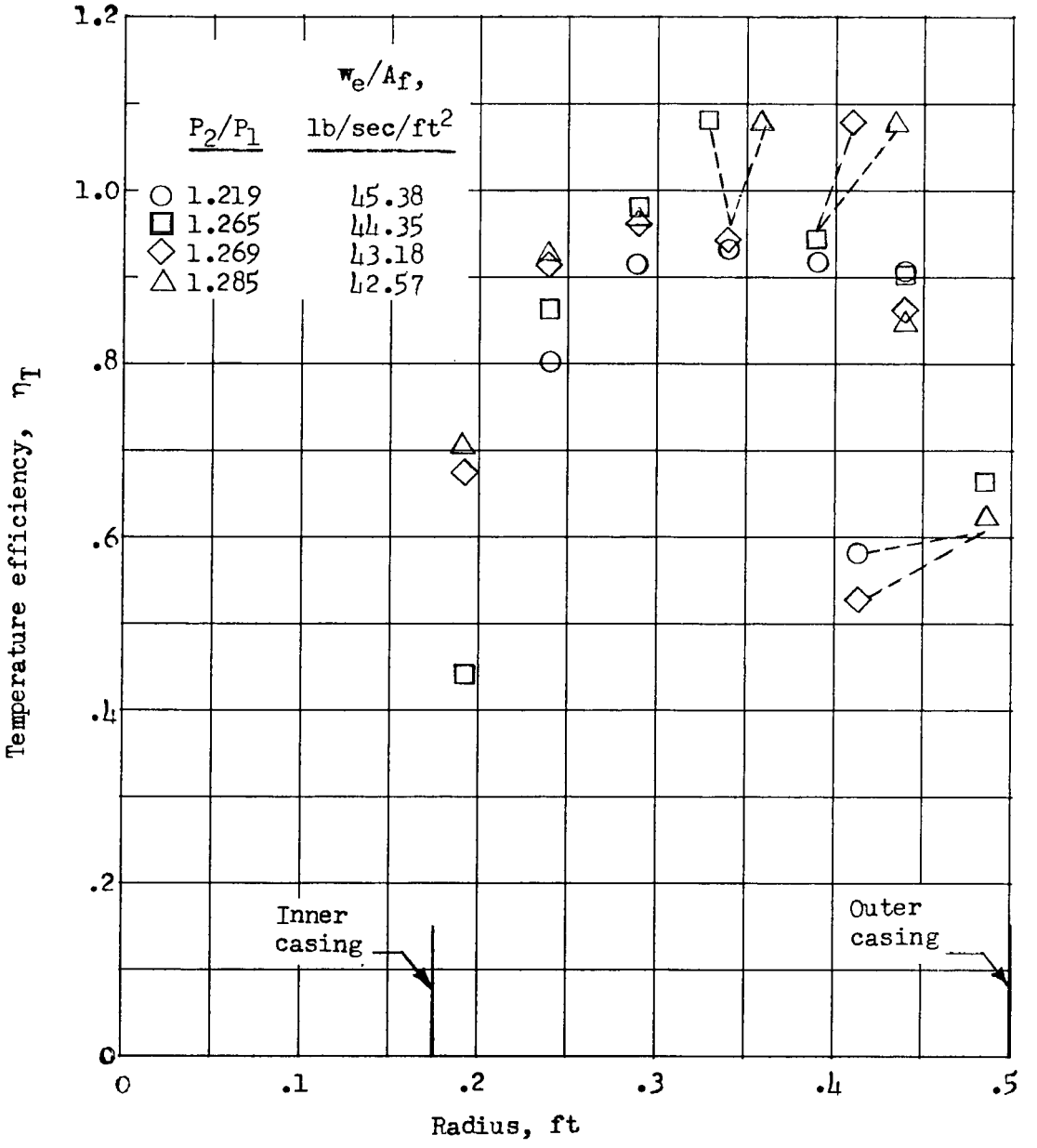

(e) Design speed.

Figure 8.- Continued.

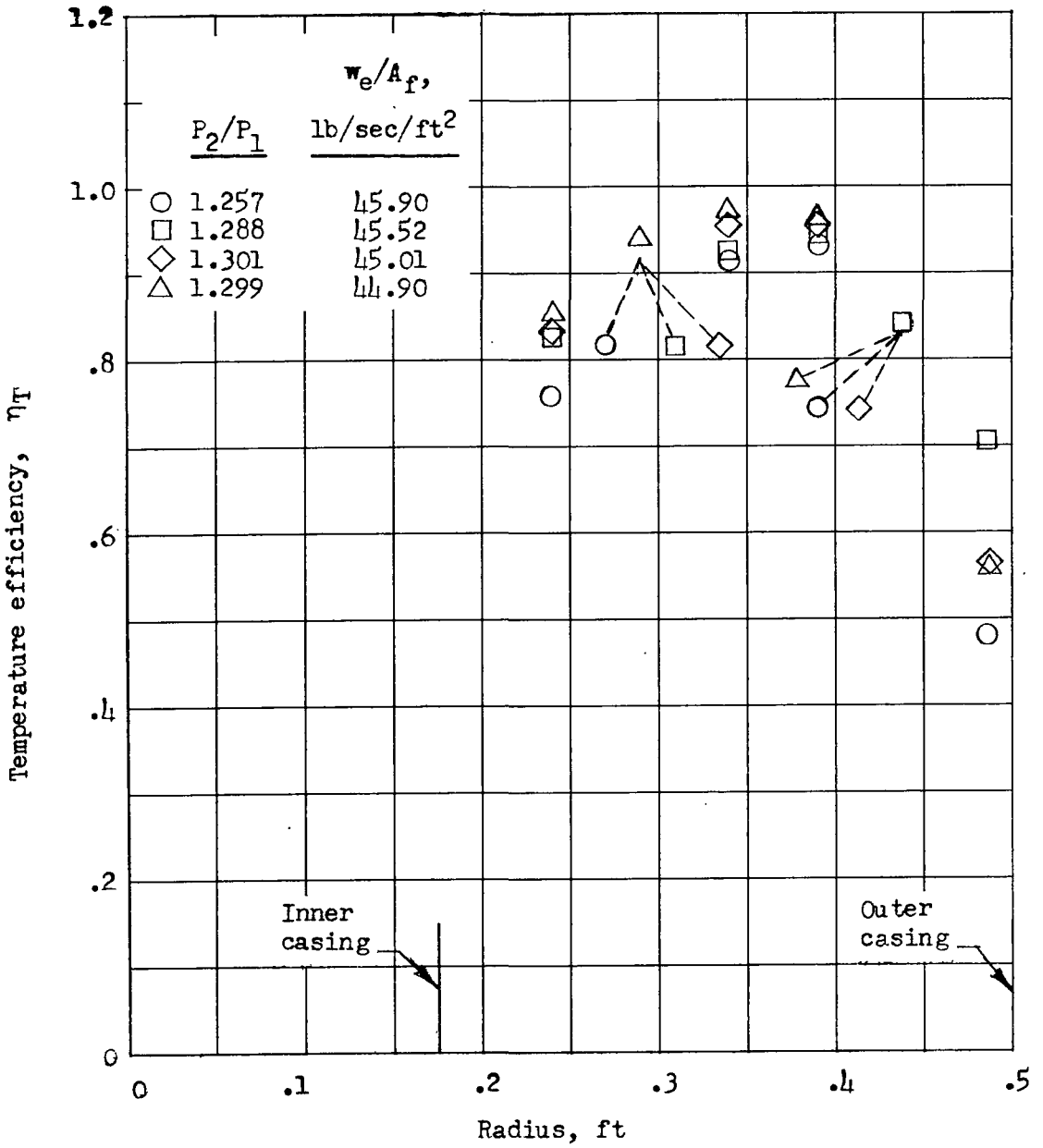

(f) 105-percent design speed.

Figure 8.- Continued.

[redacted]

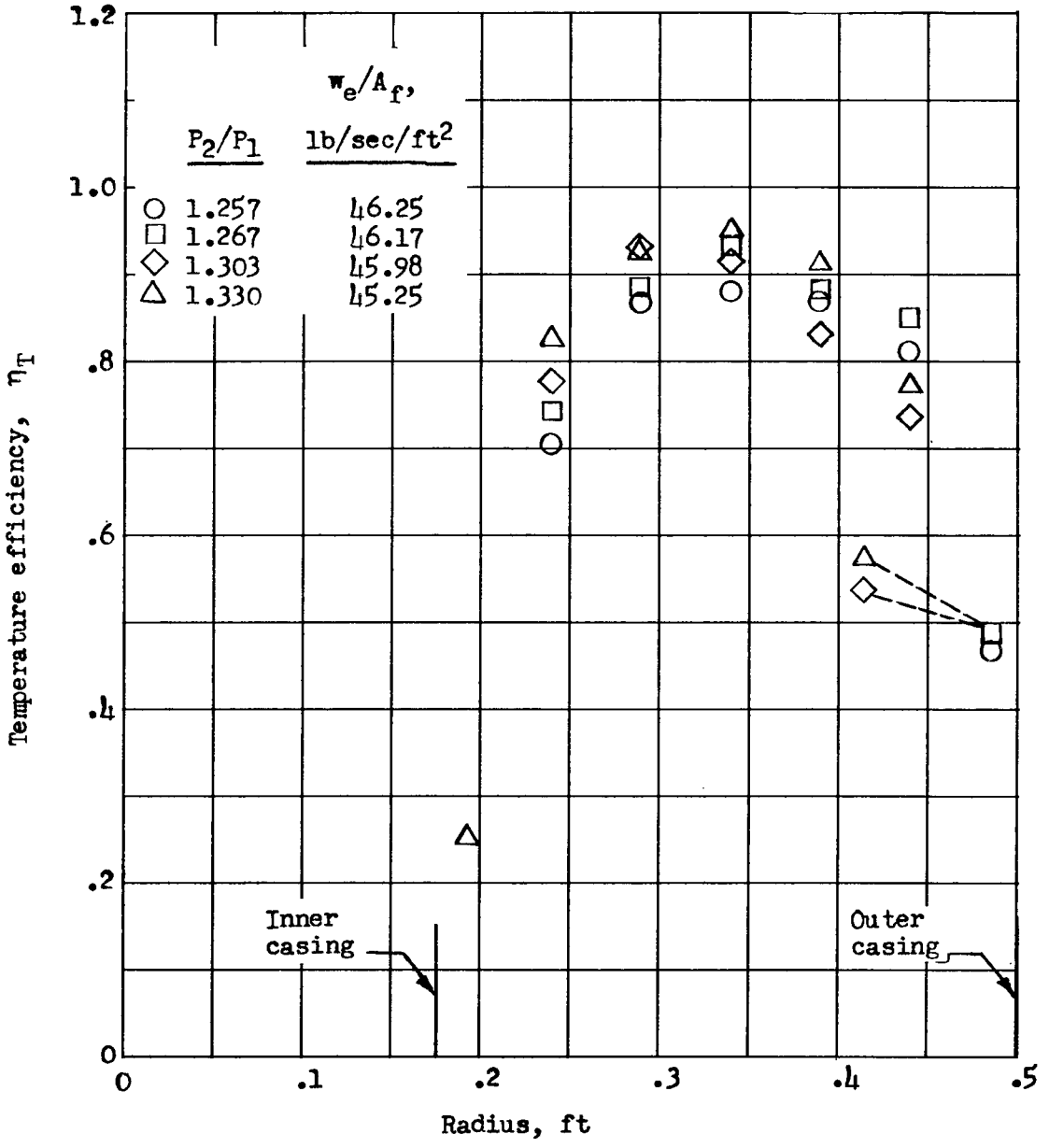

(g) 110-percent design speed.

Figure 8.- Continued.

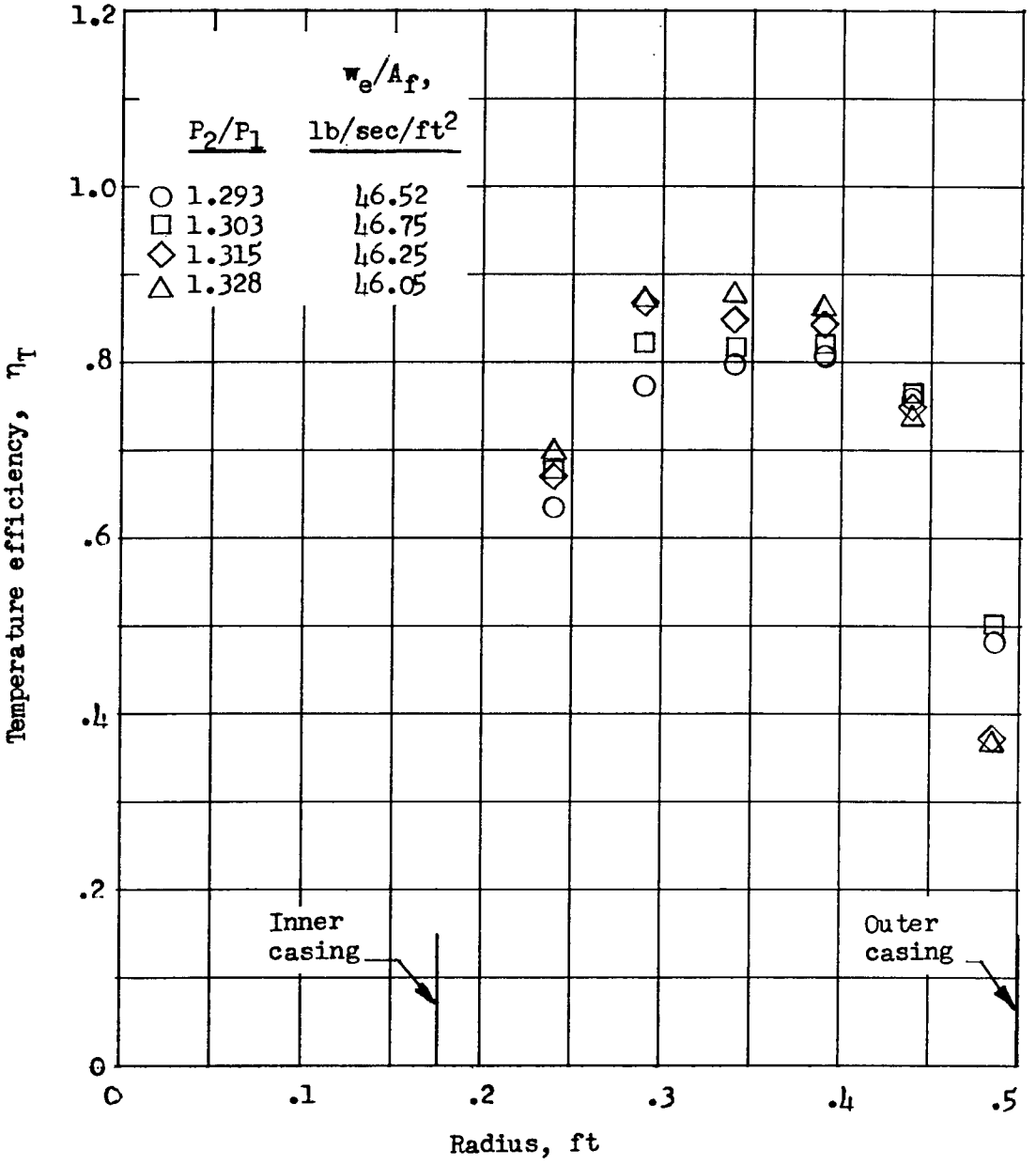

(h) 120-percent design speed.

Figure 8.- Concluded.

[redacted]

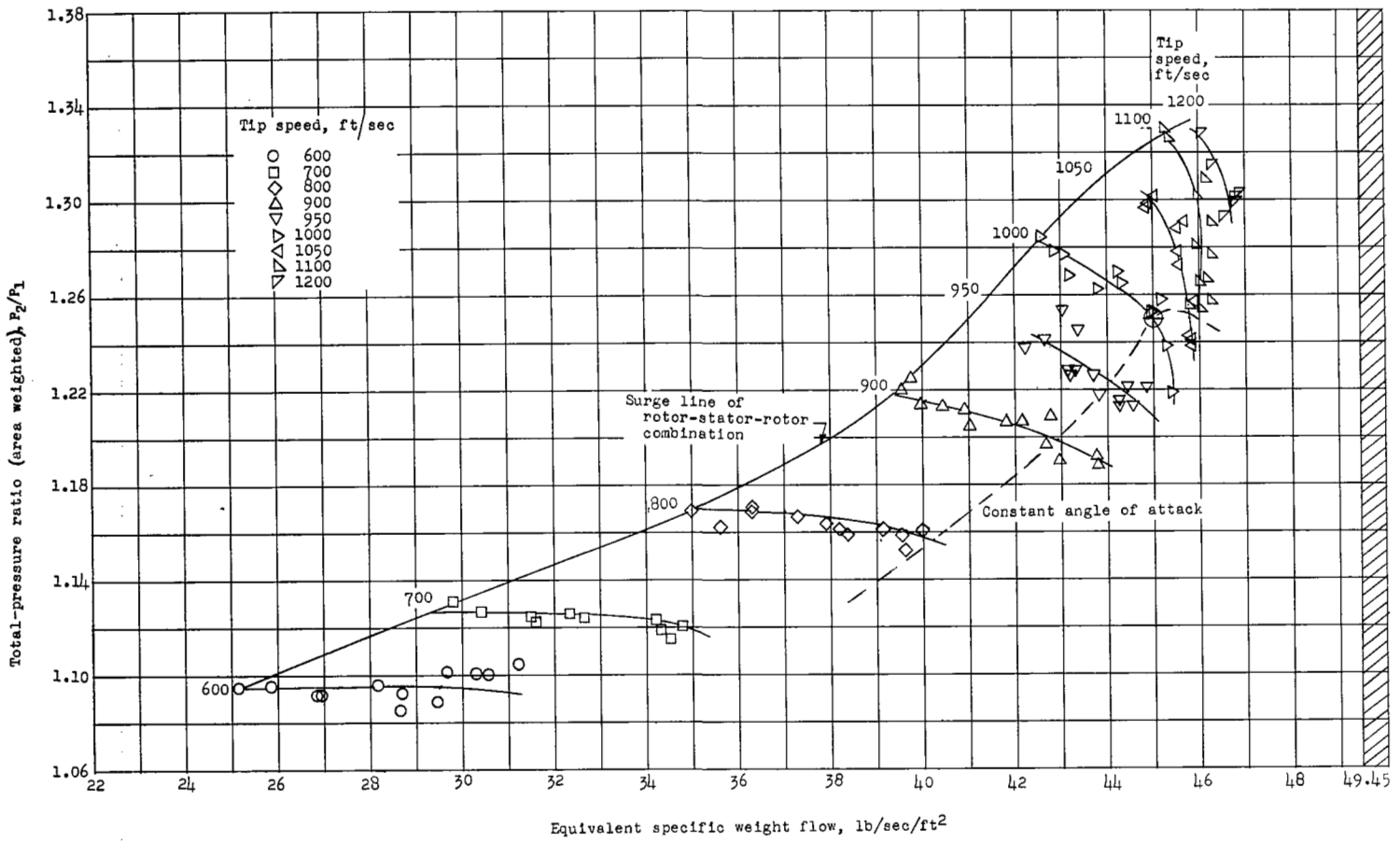

(a) Total-pressure ratio (area weighted) against equivalent specific weight flow.

Figure 9.- Overall performance of pinwheel rotor.

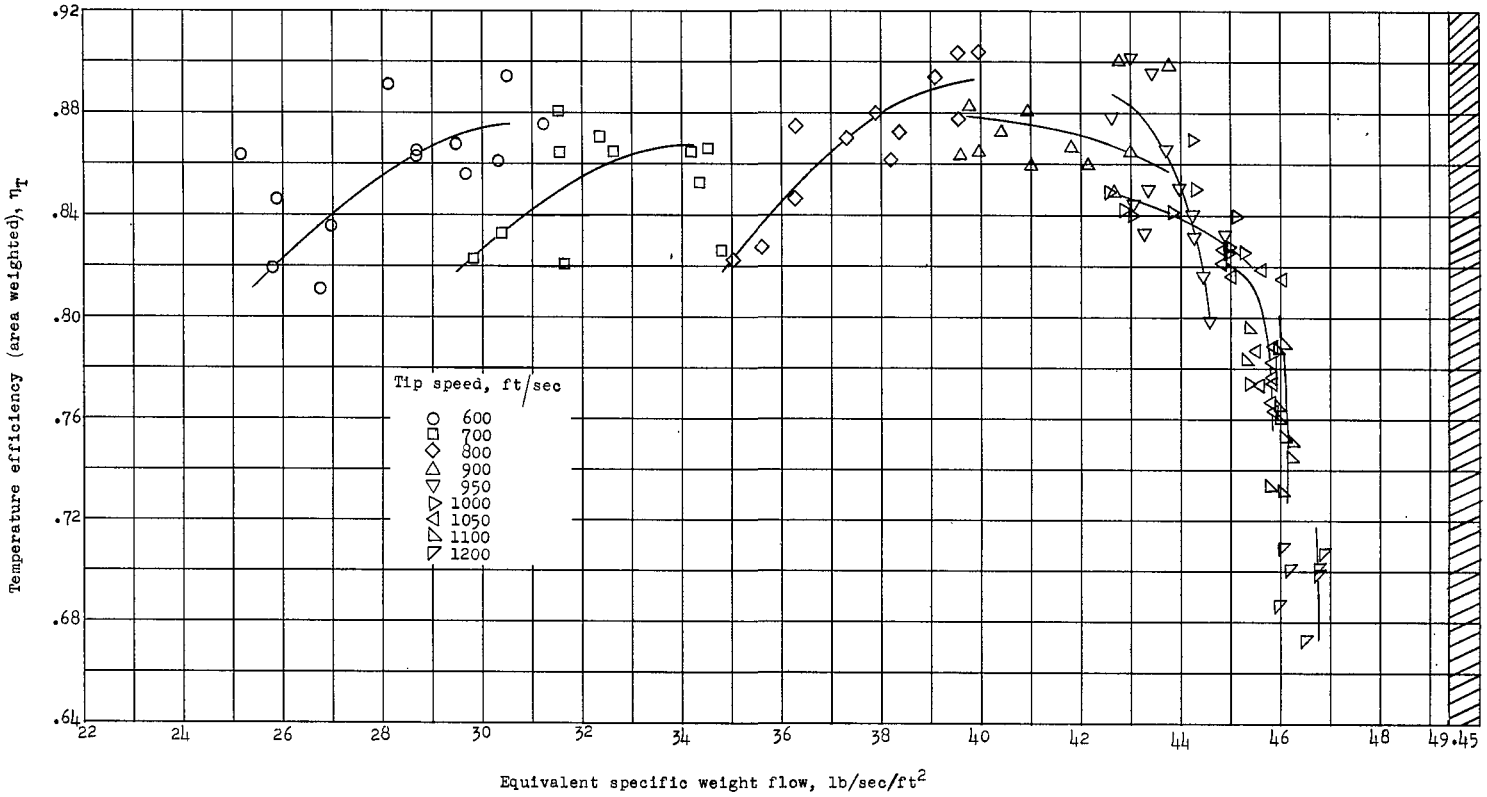

(b) Temperature efficiency (area weighted) against equivalent specific weight flow.

Figure 9.- Concluded.

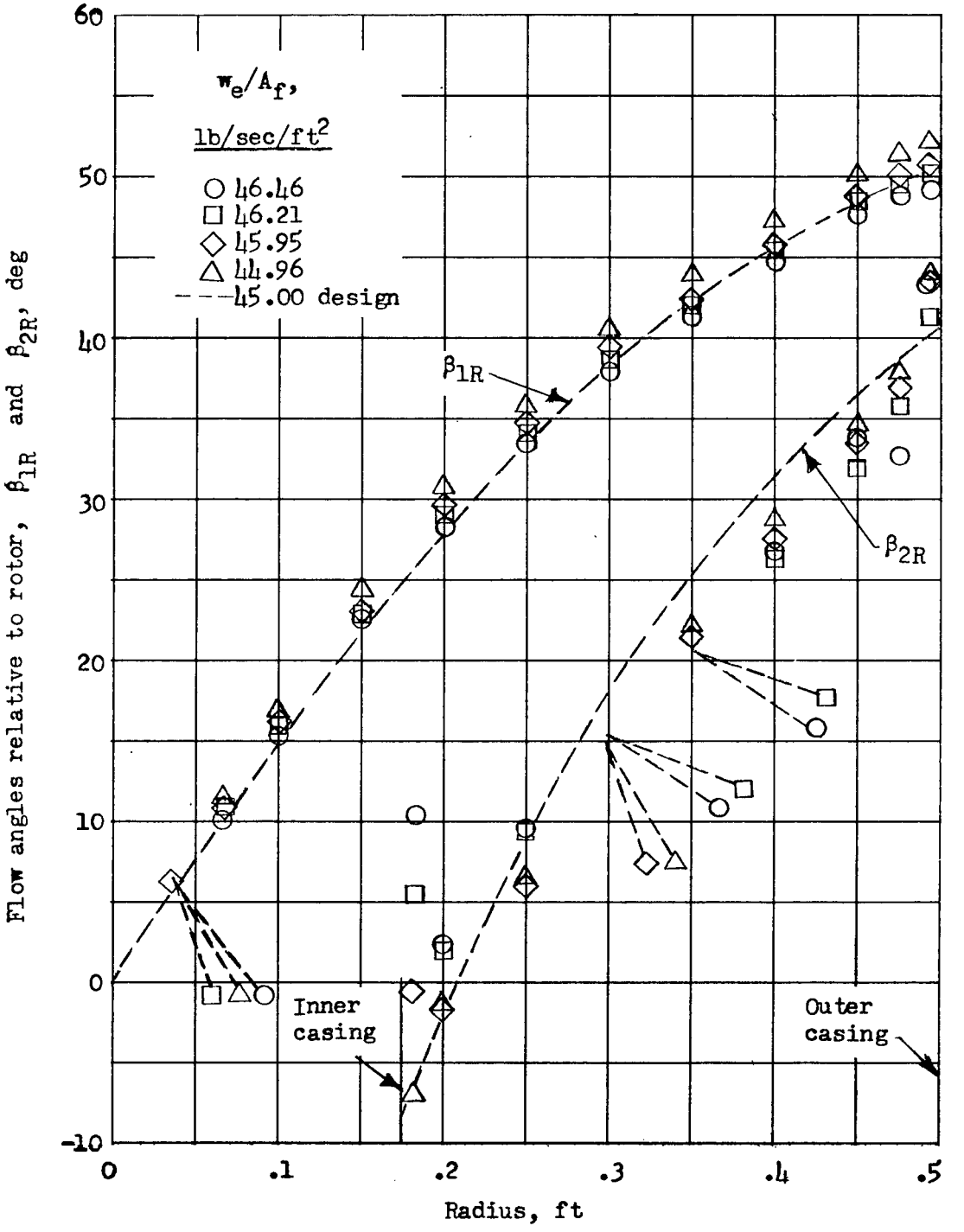

Figure 10.- Inlet and outlet flow angles relative to rotor at design speed.